Fall 2023

Pulsed Laser Deposition Approach to Metal Organic Thin Film Growth With Thin Film Developments and Applications in Electrochemical Sensing of Heavy Metal

Jacob A. Berry
Missouri State University, jacobberry@missouristate.edu

PULSED LASER DEPOSITION APPROACH TO METAL ORGANIC THIN FILM GROWTH WITH THIN FILM DEVELOPMENTS AND APPLICATIONS IN ELECTROCHEMICAL SENSING OF HEAVY METAL

A Master's Thesis

Presented to

The Graduate College of

Missouri State University

In Partial Fulfillment

Of the Requirements for the Degree

Master of Science, Materials Science

By

Jacob Berry

December 2023

PULSED LASER DEPOSITION APPROACH TO METAL ORGANIC THIN FILM GROWTH WITH THIN FILM DEVELOPMENTS AND APPLICATIONS IN ELECTROCHEMICAL SENSING OF HEAVY METAL

Physics, Astronomy, and Materials Science

Missouri State University, December 2023

Master of Science

Jacob Berry

ABSTRACT

In recent years metal organic frameworks (MOFs), have drawn a lot of attention for their vast and tunable properties. This work is an approach to solve device application issues at the interface of the crystals by introducing a thin-film approach to the self-assembly of the metal organic. The growth using Pulsed Laser Deposition to solve this issue is a novel approach to device and film development. Films have been characterized using Raman spectroscopy, Fourier-Transform infrared spectroscopy (FTIR), X-ray photoelectron spectroscopy (XPS), X-ray Diffraction, Ellipsometry, laser scanning confocal microscope (LSCM), electrical measurement. Studying the properties of the grown film to compare and extrapolate the differences between it and its bulk counterpart. In large the XPS data details the chemical state of the film and its correlation to the bulk counterpart. This work entails the process engineering and developments made to overcome a seemingly impossible task. Electrochemical devices were made on Ti/Au working electrodes and tested with cyclic voltammetry as well as square wave stripping voltammetry.

KEYWORDS: metal-organic framework, thin film, pulsed laser deposition, zirconium amino benzene-dicarboxylate, self-assembly

PULSED LASER DEPOSITION APPROACH TO METAL ORGANIC THIN FILM GROWTH WITH APPLICATIONS IN THIN FILM CAPACITORS AND ELECTROCHEMICAL HEAVY METAL SENSORS

By

Jacob Berry

A Master Thesis
Submitted to the Graduate College
Of Missouri State University
In Partial Fulfillment of the Requirements
For the Degree of Master of Science, Materials Science

December 2023

Approved:

Kartik C. Ghosh, Ph.D., Thesis Committee Chair

Ridwan Sakidja, Ph.D., Committee Member

Tiglet Besara, Ph.D., Committee Member

Julie Masterson, Ph.D., Dean of the Graduate College

ACKNOWLEDGEMENTS

Firstly, I would like to thank my advisor Dr. Kartik Ghosh for all his advice, encouragement, and guidance along the way. I would like to thank Jordan Valley Innovation Center for the use of their equipment as well as my employment. I would like to personally thank the Director of Research Rishi Patel with JIVC for his insight and help along the way. I would like to thank the U.S. Army Engineer Research and Development Center, as the funding agency for this work.

TABLE OF CONTENTS

LIST OF TABLES

LIST OF FIGURES

Chapter 1: Overview

Commonly metal organic frameworks (MOFs) have been used as bulk powder for a variety of applications such as gas storage, gas or vapor separation, luminescence, catalytic activity, luminescence, and drug delivery. The goal of this work is to develop an improved method to take advantage of the catalytic properties of Zirconium amino benzene-dicarboxylate (UiO-66-NH_2). MOFs are tunable porous structures exhibiting a wide range of properties.

In this work the development is such that producing a thin film therefore the scaffolding of the framework might have been lost. MOFs have tunable porosity which allows for variability in properties by structural changes, this has been widely studied. The tuning of the structural properties facilitates the charge dependent uptake of ions in the solution, this tuning is generally in addition to the mixture with an additional component for the use as a sensor, thus forming a composite. This, with the water and thermal stability were major considerations as to why UiO-66-NH_2 was chosen.

Physical vapor deposition is not a common approach to the development of an organic thinfilm, this could allow for high quality films to be developed. There are many obsticles that must be overcome with such an approach such as target heating, substrate heating, decomposition of the organic on either surface. Confirmation of the grown film and its phase then becomes extremely difficult with films being analyzed with X-ray photoelectron spectroscopy, fourier transform infared spectroscopy, Raman spectroscopy, X-ray diffraction, laser scanning confocal microscopy, and electrical measurements. With metal organics having a high band gap and low decomposition temperature these characterizations are extremely important in determining the quality of the film.

Films were grown on a variety of substrates; gold, silicone, silicone dioxide, and alumina. Oxide substrates are known to be the site of nucleation for metal organic growth, therefore it is interesting to prove the growth on more difficult surfaces. These surfaces are the ones that have the most potential applcations as there are very minimal applications that involve a junction of two insulators.

Figure 1.1 shows the overall workflow chart for both efforts. There is a large crossover from chapter 2 to chapter 3, due to 2 being a process development with materials growth characterization and 3 being a more in-depth application. Beginning with the synthesis of the pristine material and approach to the PLD grown MOF. Then characterization of grown films using a variety of different highly advanced techniques, including X-ray photoelectron spectroscopy, X-ray diffraction, Raman spectroscopy, Fourier transform infrared spectroscopy, electrical measurements, and dielectric constant. Into the latter part of the application in an electrochemical device. Working electrodes were manufactured via titanium and gold sputtering with the PLD grown MOF on the target of the electrode. The MOF grown for the with the modified method which proved to be a more likely method for the growth of the correct structure and chemical composition, both of which are novel approaches for the growth of a thin film MOF. Cyclic voltammetry and square wave stripping voltammetry were done on electrodes, although they show some errors with the fabrication method of the electrochemical electrodes. Fourier transform infrared spectroscopy was measured on the deposited electrode to confirm the growth of the MOF when compared to the other non-electrode samples.

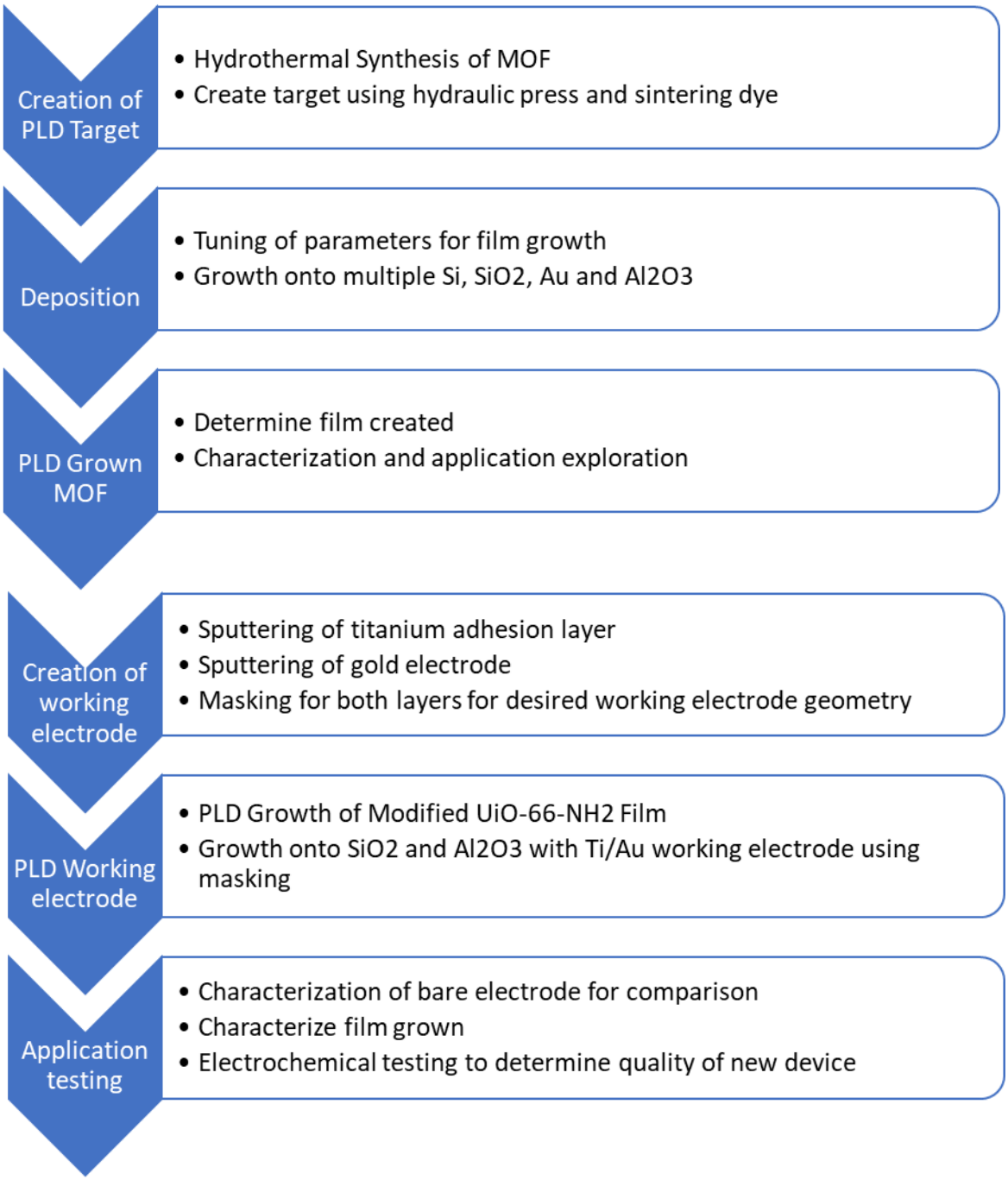

Figure 1.1: Workflow chart containing an overview of both chapter 2 and 3.

Chapter 2: Pulsed Laser Deposition of UiO-66-NH_2

Abstract

This study is an important step toward developing novel thin film metal-organic frameworks (MOFs). UiO-66-NH_2 was chosen due to its thermal, mechanical, and chemical properties, likely giving the greatest probability of success. Using pulsed laser deposition at 100°C in an inert environment at a lower energy density was used. This work contains two different approaches to growing the film, the latter of which X-ray photoelectron spectroscopy (XPS) shows is more like the composition of the pristine film. Multiple substrates were used successfully, although, ones with the most applications were chosen. X-ray diffraction (XRD), film thickness via laser scanning microscopy, Fourier transform infrared spectroscopy (FTIR), Raman spectroscopy, and electrical measurements were used to characterize both grown films and throughout the process.

Introduction

Metal-organic Frameworks (MOFs) are an emerging group of materials with promising applications in chemical sensing [1,2], energy storage [3], electrodes [4], separators [5], electrolytes [6], drug delivery [7] and potentially more. Having a material with a high surface area [8] that is tunable with pores that are equally tunable by the pour environment. Zirconium-based MOFs show promise for applications due to their inherent chemical and thermal stability [9,10]. With such a variety of applications and high potential it is easy to understand why MOFs are being heavily studied currently and in recent years.

UiO-66-NH2 is a well-studied metal organic framework with a large variety of application possibilities. Many attempts have been made to make uniform high-quality metal

organic thin film for those applications. A MOF can be defined as hybrid organic-inorganic solid having porosity [11]. Many approaches have been tried to make this such as liquid-phase epitaxy [12], Langmuir-Blodgett layer by layer deposition [13], in-situ crystallization [14], growth at room temperature [15], dip coating in mother solution [16], slow diffusion of reactants [17], Electrochemical [18]. Some of the methods were to develop single crystal, polycrystalline, or 2-dimensional MOFs as thin film. It is also important to note that different growth methods can form different phases.

The properties of the material for this novel development were chosen to give the highest probability of success. Key considerations were the thermal and chemical stability of the MOF, UiO-66-NH_2 having both of those characteristics [10]. Next is the mechanical rigidity of the MOF in question in which UiO-66-NH_2 possesses these properties as well [19]. These being the main keys for a material to make it through the entirety of the process.

To current knowledge pulsed laser deposition has not been used to develop any metal organic framework films. It has been used to develop polymer [20], metal, and metal-oxide, nitrides, carbides films [21]. Some of the differences being in the energy density of the applied laser, as well as the wavelength of that laser. The deposition environment and temperature of the substrate can also be varied for the desired application.

Experimental Method

Pristine UiO-66-NH_2 Powder used was prepared from a hydrothermal procedure with minor modification [1]. ZrCL4 0.3498g, 2-NH_2-Benzenedicarbolate 0.2718g, 75mL N,N-Dimethylmethanamide (DMF), mixed in a 100mL Teflon lined autoclave. All purchased from Sigma Aldrich. The autoclave was heated in an oven for 48 hours at 120°C, then set to cool to

room temperature before opening. The solution was centrifuged at 10,000rpm for 10min with the supernatant removed between washes of ethanol to remove residual precursors. The precipitate was then vacuum dried for 12 hours at 100C.

One inch diameter Pulsed Laser Deposition targets were produced by sintering them in a hydraulic press. 20,000 psi in a hydraulic press the sintering die was coated with Chemlease R+B EZ Release Agent to create a nonstick surface. The goal thickness was 2-3 mm with as high density as achievable. The diameter of the target was one inch. This sintered target was mounted to a target holder.

Pulsed laser deposition, for growth of the MOF used the manufactured target on the selected substrates. Samples sizes were approximately 5mm×5mm with thickness being substrate dependent. Deposition was done with a substrate temperature of 100℃, in an inert environment of Argon at a pressure of 0.001 mbar, followed a base vacuum of approximately 1×10^{-6} mbar. These parameters were used for all substrates, as well as both the pristine and modified targets. The films were deposited using a solid state Quantel ND: YAG laser with a 266nm wavelength, thus emitting photons in the fourth harmonic. A repetition rate of 10Hz with a pulse width of 150μs and a FL-Q switch Delay of 140μs, thus giving a 1.2mW pulse with a spot size of 0.2236 cm^2. The substrate was placed on the substrate holder 30mm from the surface of the target. For this set up the incident beam is focused on the target with an angle of 60º normal to the surface. 10,000 shots were used to grow the film with an additional 500 shots to remove any contamination from the surface of the target. Prior to deposition all substrates were thoroughly cleaned with methanol and deionized water, with sonication in methanol and rinsing with deionized water.

UiO66-NH_2 metal organic thin film grown on multiple substrates were tested: alumina, silicon, silicon dioxide, and gold. Silicon and Gold [15] are to be used for device applications. In coordination with literature Al_2O_3 [3], the nucleation sites for UIO66-NH_2 are on metal oxides.

For resistance measurements a 4-point probe method was used to acquire the sheet resistance of the film, this was performed on insulating substrates to avoid shorting the film. A parallel plate capacitor method was used measuring capacitance of the grown films. The bottom electrode being either gold or conductive silicon, sample dependent. The top electrode was gold sputtered gold, using a mask for deposition, this allowed for uniformity across all samples. Onto of the gold electrode silver paste was dried so as not to puncture the 100nm gold film.

Results and Discussion

Formation of the target is somewhat of a difficult process, due to sticking to the sintering dye causing the target to break. The carbonization of the surface and potentially into the target, this structural change would make the formation of the same material onto the substrate thereby changing the Material form the MOF to a carbon rich metal oxide structure.

The targets coming from the press were measured to confirm their thickness, volume, and density. There was some loss from the initial mass to their mass post sintering, this correlation could not be made due to some loss of powder being lost in the process. Table 1 shows data for the creation of targets with mass, thickness, volume, and density calculated or measured. Volume and thickness were measured with a Keyence VR series One-shot 3D. Using an optical 3d macroscope to map the target was determined to have less error than a caliper measurement due to the roughness and edges of the target. Mass was measured on a microbalance. Density calculations are simply a function of mass per unit volume. The density for the UiO-66-NH_2

target can be compared to the theoretical density for the MOF to have an idea of the packing density of the target. With a theoretical density of 1.237 g/cm3 [22] the density of the target is exceptionally close, a percentage difference of 0.3234%. The modified target has a percent difference of 0.8407%, with that said it cannot be used for comparison due to the high percentage of 2-Aminoterephthalic acid. There is the possibility that some of the perceived gain in density for the target is in fact due to the carbonization of the organic portion of the MOF in the sintering process.

Table 1: Target creation for PLD

Target	Mass	Thickness(mm)	Measured Vol(cm3)	Density
UIO66-NH2	0.8057	1.327	0.65355	1.232805
ModifiedUIO66-NH2	0.8335	1.056	0.6795	1.226637

X-ray powder diffraction was performed with a Bruker D2 Phaser instrument with $CuK\alpha_2$ radiation (λ = 1.5406 Å), powder samples were run on zero background silicon substrates. Powder being dispersed in doubly deionized water then drop cast onto the substrate. The water was removed by drying on a hotplate at 100°C for 30 minutes. The UiO-66-NH_2 mixture from the target was checked such that the stability of the structure was preserved after the sintering process was completed Figure 2.1 (a). The mixture UIO-66-NH_2 is a 50% MOF and 50% 2-Aminoterephthalic acid shown in Figure 2.1 (b). Pristine UIO-66-NH_2 was grown and matched very well with literature shown in figure 2.1 (c). This is talked about later in the XPS data as to why this decision was made. This confirmation held true for all the sintered targets.

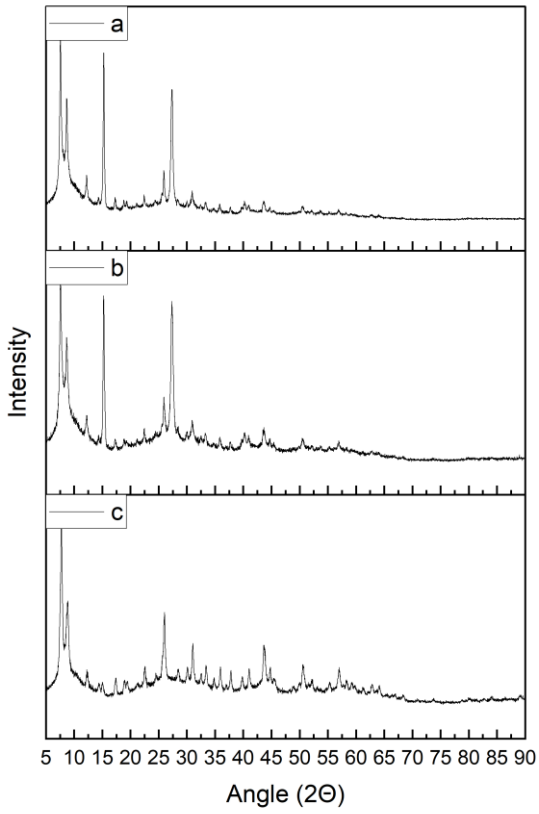

Figure 2.1: Powder X-ray diffraction. (a) UiO-66-NH_2 scraped from the mixed target, (b) UiO-66-NH_2 mixture sintering, (c) pristine UiO-66-NH_2 as synthesized.

XRD of the thin films proved to be difficult and nearly inconclusive for the grown films with only the substrate peaks showing through. The amorphous region from about 5-15 deg 2-Theta shown below in figure 2.2. This shows that this method produces potentially amorphous film even when grown at the best parameters yet known. Which correlates with other film growths at lower temperatures generally being amorphous. This is the case for both UiO-66-NH2 films as well as films grown from the mixed target. This proved to be the case for all temperatures tried for the growth.

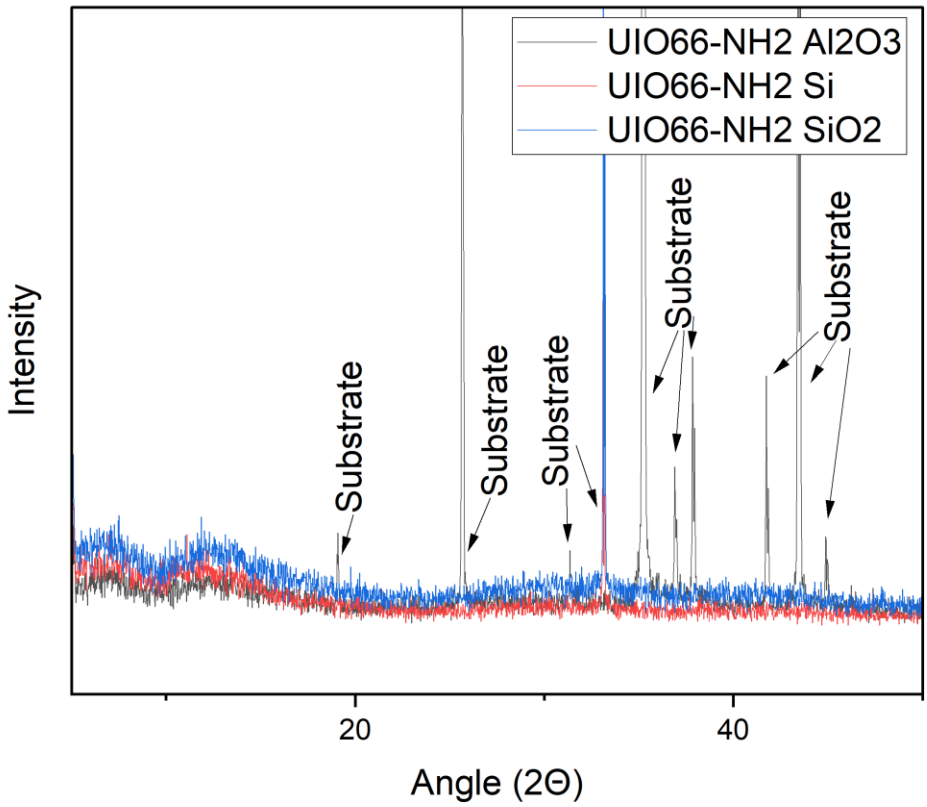

Figure 2.2: Powder X-ray diffraction of an overlayed plot of the MOFs grown with PLD on 3 different substrates.

X-ray Photoelectron Spectroscopy (XPS) was performed with a Thermo Scientific™ Nexsa G2 X-ray photoelectron spectroscopy, to get an understanding of both the composition and the chemical bonds of the films. Peak shifting compensation was accounted for with the use of a flood gun, note that the argon bombardment of the film can cause a reduction in the zirconium oxide, to overcome that the minimum potential was used. Accounting for that a survey was run followed by subsequent surveys minimizing the shifting as a function of the energy, it turned out that only 0.1V potential was required for the flood gun to compensate the surface charge for these films. Powder films were analyzed by drop casting the powder in post sonication

in water drying it to a silicon wafer to be inserted to the instrument. Figure 2.3 (a) below shows the XPS survey scan containing the entirety of the range of 1350 to -10 eV for the five scans that were taken in a 400-micron area with an increment of 200 eV and a resolution of 0.1 eV, these parameters were used for all survey scans. This scan shows the chemical constituents of the starting material. It is important to note that the surface of the deposited film was etched away to remove surface contaminants allowing for a more accurate examination of the material in question. The pristine scan contains some chlorine and fluorine that was likely a contamination of the deionized water used to wash and suspend the samples. The information in figure 2.3 (b), the atomic percentage comes into play greatly as it is the chemical composition of the material trying to be recreated.

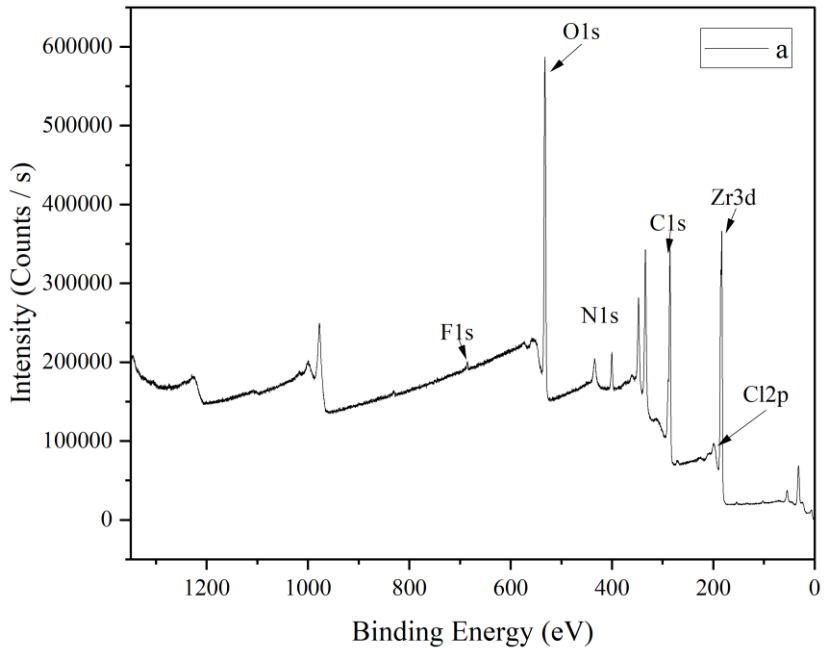

(b)

Name	Peak BE	FWHM eV	Area (P) CPS.eV	Atomic %
O1s	532.17	3.5	1562298.55	32
Zr3d	183.41	4.39	1415950.84	7.29
C1s	285.35	3.05	1036477.64	51.32
N1s	400.09	3.11	164650.17	5.25
Cl2p	197.54	7.3	178543.39	3.05
F1s	685.51	3.27	66684.46	1.09

Figure 2.3: XPS of Pristine UiO-66-NH_2 (a) XPS Survey Scan for Pristine powder grown hydrothermally, (b) Table containing the atomic composition of the Pristine powder.

Continuing to the high-resolution scans for the XPS spectra of the powder in figure 2.4. The difference between the high-resolution scan and the survey scan is the spacing change to 0.01eV for the region of interest. The high-resolution scans binding energy directly correlates to the valence electrons and their occupied state. Figure 2.4 (a) is the Zr 3d scan that contains both the 3d 5/2 and 3/2 both of which the binding energy match for that of the ZrO_2 which correlates to XRD spectra matching for the structure. The O1s scan in figure 2.4 (b) has binding energies ZrO_2, C-O, and C=O with C-O being the linker between the ZrO_2 and the carbon structure. Interestingly the C1s scan in figure 2.4 (c) predominantly C-C or C-H bonds which correspond to the structure of the organic portion of the MOF. In figure 2.4 (d) the N1s scan shows the amine functional group that coordinates to the NH_2 in the MOF, this specific functionalization is for electronegativity giving advanced properties. Figure 2.4 (e,f) are contaminants shown that are from the water in the solution and from the salt used in the production of the MOF. In Table 2, all the high-resolution scans are compiled into a more digestible format. This compilation of the

high-resolution data gives an insight to the chemical makeup of the MOF. Deconvolution was done on all high-resolution scans using the Avantage software provided by Thermo Scientific. Peak positions for chemical state analysis were done using the NIST database for reference information.

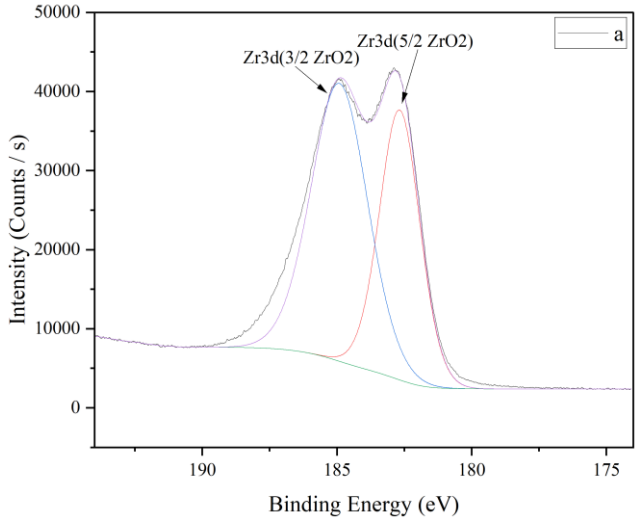

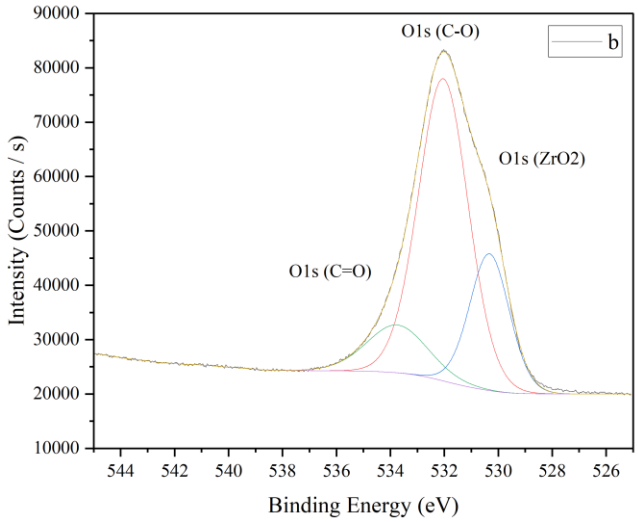

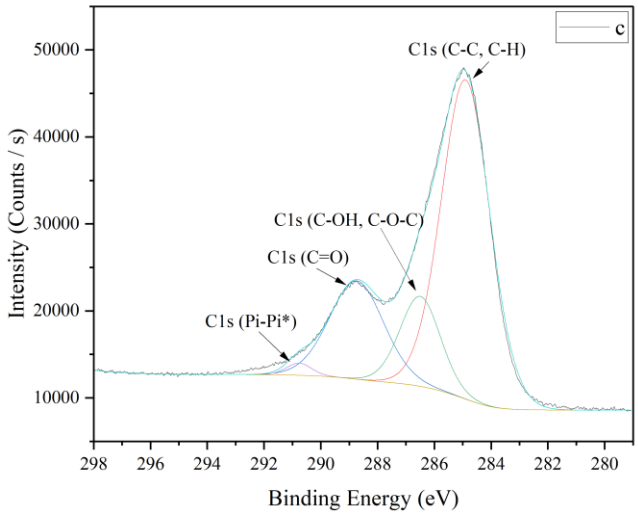
c
C1s (C-C, C-H)
C1s (C-OH, C-O-C)
C1s (C=O)
C1s (Pi-Pi*)
Intensity (Counts / s)
Binding Energy (eV)
50000
40000
30000
20000
10000
298
296
294
292
290
288
286
284
282
280

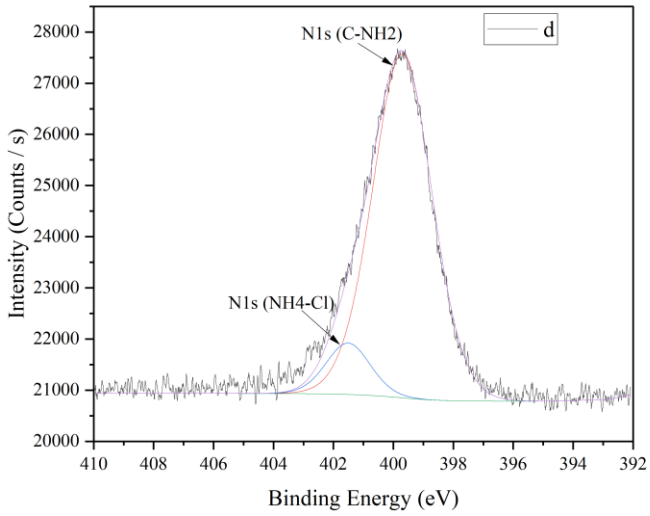
d
N1s (C-NH2)
N1s (NH4-Cl)
Intensity (Counts / s)
Binding Energy (eV)
28000
27000
26000
25000
24000
23000
22000
21000
20000
410
408
406
404
402
400
398
396
394
392

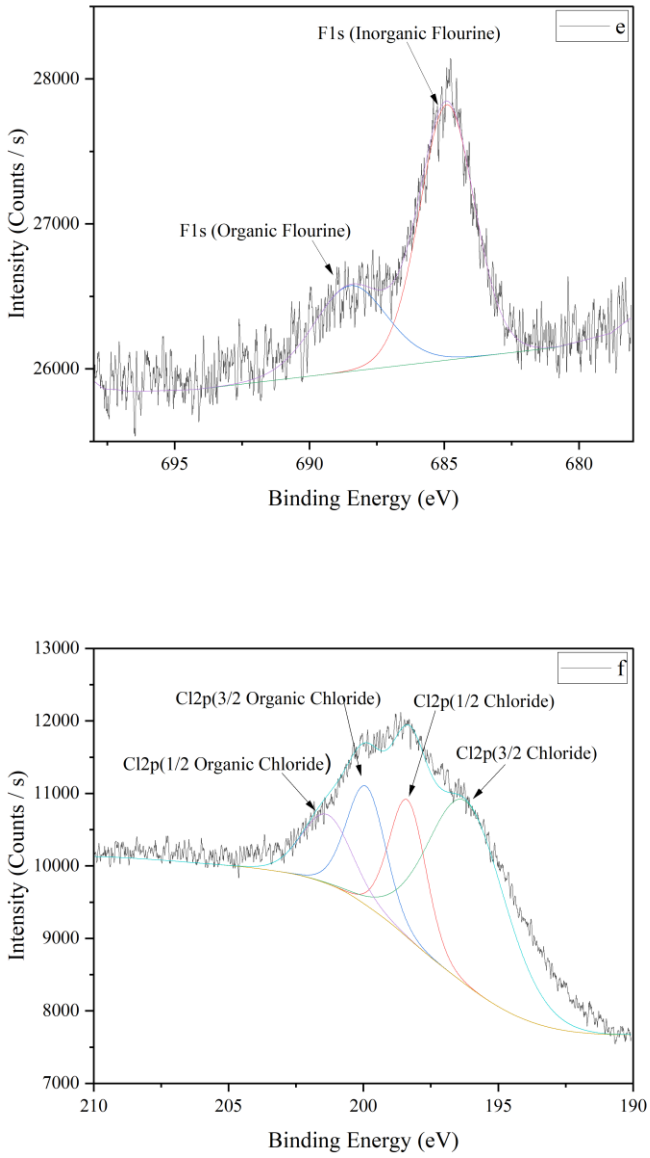

Figure 2.4: High-resolution XPS Scans of UiO-66-NH_2 Pristine powder (a) Zirconium 3d, (b) Oxygen 1s, (c) Carbon 1s, (d) Nitrogen 1s (e) Fluorine 1s, (f) Chlorine 1s.

Table 2: High-resolution XPS scans for Pristine UiO-66-NH_2 tabulated for Figure 2.4 (all)

Name	Peak BE	FWHM eV	Area (P) CPS.eV	Atomic %
Zr3d (5/2 ZrO2)	182.67	1.77	65369.54	2.72
Zr3d (3/2 ZrO2)	184.91	2.47	94215.27	3.92
Cl2p(3/2 Chloride)	196.2	3.36	9218.04	1.27
Cl2p(1/2 Chloride)	198.36	1.61	3311.94	0.46
Cl2p(3/2 Organic Chloride)	199.9	1.7	3029.46	0.42
Cl2p(1/2 Organic Chloride)	201.35	2.2	2274.04	0.32
C1s (C-C, C-H)	284.93	1.99	82138.94	32.86
C1s (C-OH, C-O-C)	286.53	1.56	17174.08	6.88
C1s (C=O)	288.74	2.25	27578.16	11.06
C1s (Pi -Pi*)	290.77	1.04	1579.83	0.63
N1s (C-NH2)	399.76	2.33	16982.8	4.38
N1s (NH4Cl)	401.51	1.73	1883.43	0.49
O1s (ZrO2)	530.32	1.73	47259.44	7.81
O1s (C-O)	532.04	2.18	131152	21.71
O1s (C=O)	533.75	2.66	25363.13	4.2
F1s (Inorganic Fluorine)	684.9	2.4	4575.5	0.6
F1s (Organic Fluorine)	688.49	3.18	2038.25	0.27

The PLD growth of the MOF was done on the AL_2O_3, Si, SiO_2, and gold. The gold was sputtered onto Al_2O_3 and SiO_2 with a thickness of 100nm.Figure 2.5 (a) showing a successful survey scan of UiO-66-NH2 grown onto Silicon. Referring to the in the carbon percentage is 34% that in comparison to the 51% in Figure 2.3 (b). This differential in the pristine versus the grown UIO-66-NH2 was the reasoning for the additive to the target. The ratio that the change would need to be to theoretically accomplish this task is 1.5 times more carbon form the PLD grown to the pristine. Thus 1.5 times the mass of UiO-66-NH_2 was used for the mass fraction of 2-Aminoterephthalic Acid, which is the precursor for the pristine MOF. Notice that there is an equal ratio of nitrogen missing from the structure as well, thus why that chemical structure was chosen as the additive rather than a simpler carbon structure.

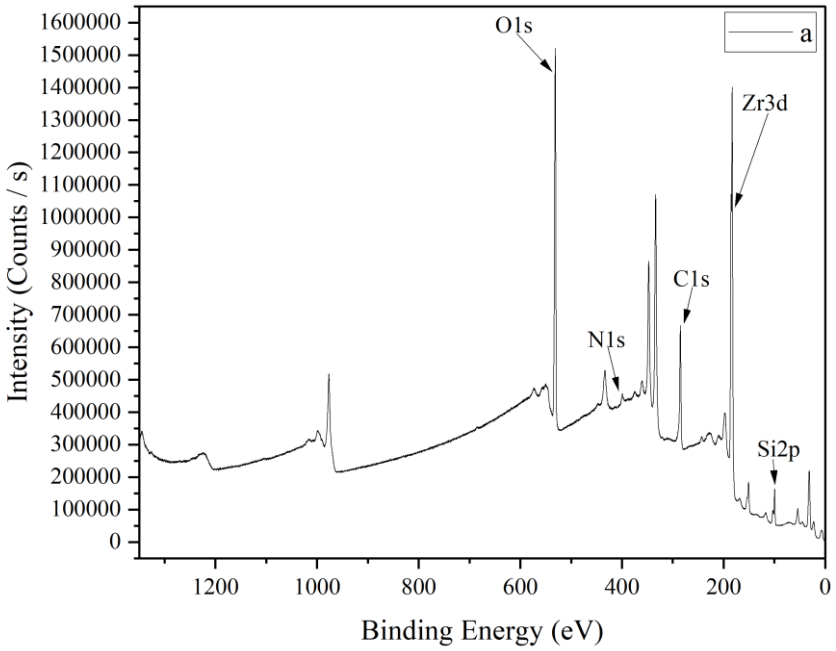

(b)

Name	Peak BE	FWHM eV	Area (P) CPS.eV	Atomic %
Si2p	99.4	1.95	330046.61	9.35
Zr3d	183.07	2.84	4813142.13	14.26
C1s	284.83	2.6	1202873.42	34.27
N1s	399.11	2.83	108628.69	1.99
O1s	531.1	2.7	3407537.46	40.13

Figure 2.5: (a)Survey Scan of UiO-66-NH_2 PLD on silicon substrate, (b) data table for the survey scan

Figure 2.6 (a-d) shows the high-resolution scans for the PLD grown UiO-66-NH_2 from the non-modified target. There is a presence of suboxide in figure 2.6 (a) which shows the Zr3d scan, this reduction is from the plasma etch that removes surface contamination. The C1s scan in figure 2.6 (b) proves to be comparable to that of the pristine material. The N1s scan in figure 2.6 (c) shows the presence of the amine group as well as the derivative of it due to the loss in the

plasma. In figure 2.6 (d) the O1s scan proves to be marginally different from the pristine high-resolution scan where the ZrO_2 peak in relation to the C-O is flipped. This is likely due to the loss of CO and CO_2 in the PLD plasma as gas pulled out by the turbo molecular pump.

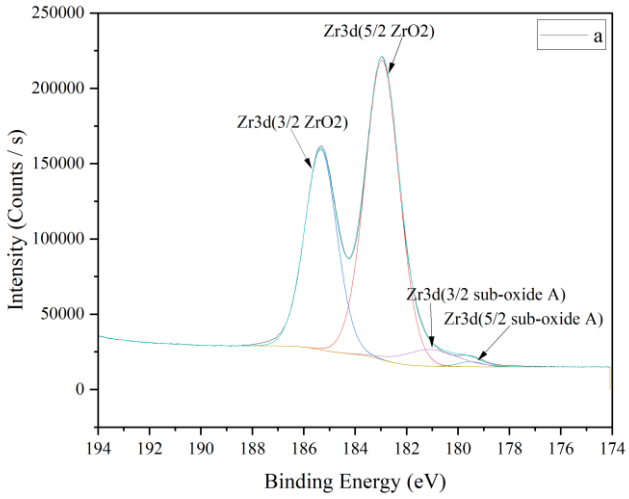

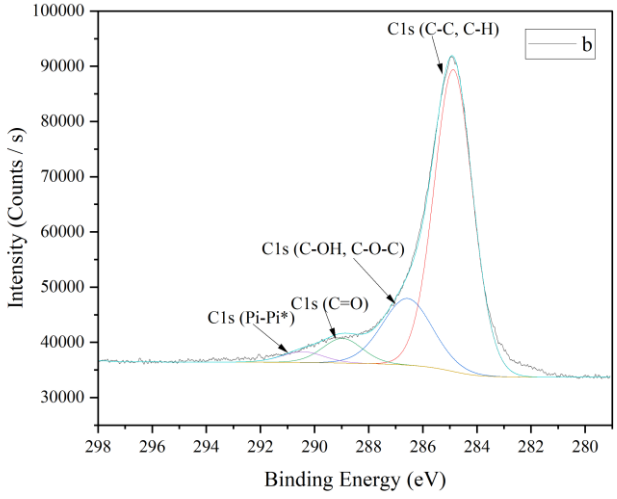

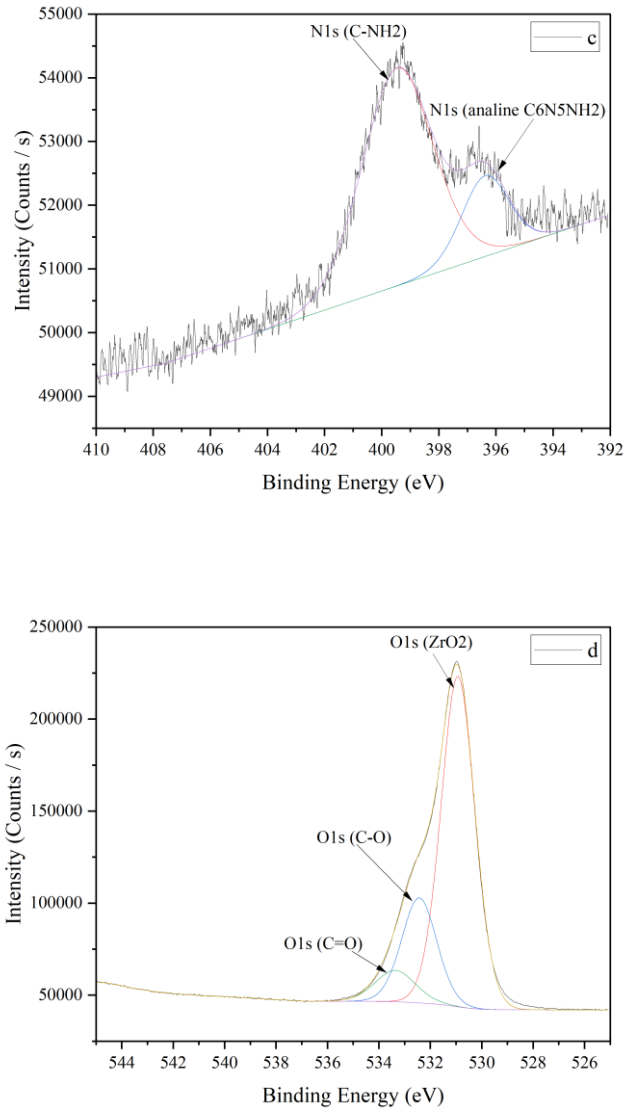

Figure 2.6: XPS high-resolution scan of UiO-66-NH_2 PLD film (a)Zr3d scan with deconvolution, (b) C1s scan with Deconvolution, (c) N1s scan with deconvolution, (d) O1s scan with deconvolution.

Table 3 below contains the deconvolution data from figure 2.6 (a-d). These values are comparable to that of the pristine MOF although there are some inherent differences. The Oxygen peak has a different ratio, The carbon content of the film is different. Both of those

differences contribute to the changing atomic percentage of the Zirconium present in the film. Although this film could have many applications it is not the goal of this work.

Table 3: High-resolution scan UiO-66-NH_2 deconvolution tabulated.

Name	Peak BE	FWHM eV	Area (P) CPS.eV	Atomic %
Zr3d (5/2 sub-oxide A)	179.52	1.11	4077.14	0.11
Zr3d (3/2 sub-oxide A)	181.07	2.41	28916.29	0.77
Zr3d (5/2 ZrO2)	182.95	1.57	338078.24	9.02
Zr3d (3/2 ZrO2)	185.33	1.46	211348.67	5.65
C1s (C-C, C-H)	284.87	1.68	99700.13	25.59
C1s (C-OH, C-O-C)	286.57	2.17	28449.24	7.31
C1s (C=O)	288.97	1.74	8439.96	2.17
C1s (Pi -Pi*)	290.44	1.83	3866.1	1
N1s (aniline C6H5NH2)	396.38	1.95	2675.85	0.44
N1s (C-NH2)	399.45	2.93	10851.53	1.79
O1s (ZrO2)	530.92	1.55	301416.79	31.98
O1s (C-O)	532.43	1.6	99309.5	10.55
O1s (C=O)	533.36	1.85	34121.21	3.63

Figure 2.7 (a) shows the survey scan of the modified target PLD and tabulated into Figure 2.7 (b). Comparison of this data with the pristine MOF shows that it is more similar compared to the nonmodified PLD. Having a carbon content of 52% and a Nitrogen content of 3.66%, compared to the 51% carbon and the 5% nitrogen for the pristine shown in Figure 2.3 (b). The ratio of the 1.5 times additive to MOF proves to produce a film more closely in composition to the pristine than that of the PLD from the MOF only.

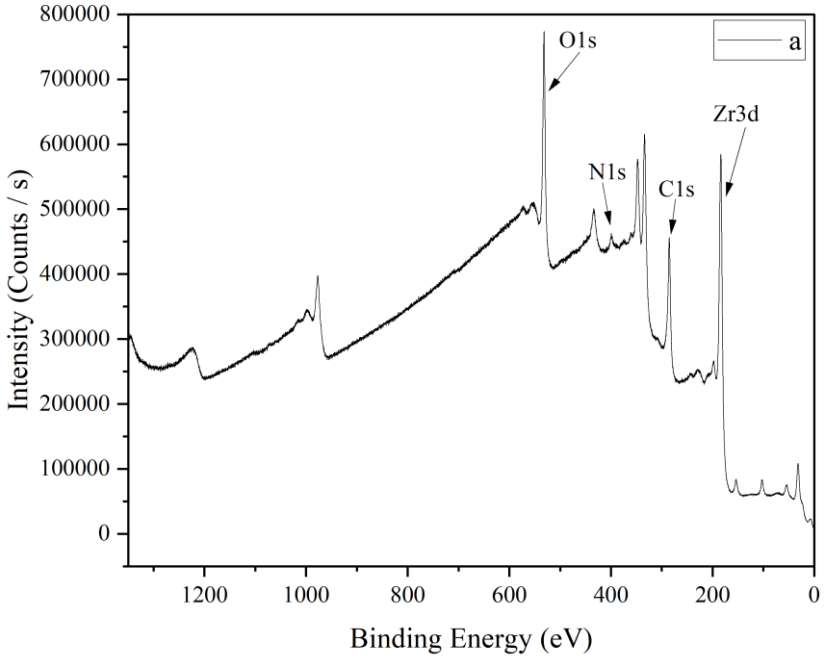

(b)

Name	Peak BE	FWHM eV	Area (P) CPS.eV	Atomic %
Zr3d	183.41	5.78	2394136.96	11.23
C1s	284.95	5.04	1160543.14	52.33
N1s	399.36	5.11	126725.92	3.68
O1s	531.45	4.71	1756621.26	32.76

Figure 2.7: XPS Survey scan of Modified UiO-66-NH_2, Modified with UiO-66-NH_2 1.5 times by mass additive of 2- Aminoterephthalic Acid (a) Survey Scan on Si/SiO_2 sputter coated with Au, (b) data table for the survey scan in figure part a

The high-resolution scans of the modified film prove to be exceptional as well. Figure 2.8 (a-d) shows the high-resolution for the film. The Zr3d scan shows predominantly ZrO_2 which directly correlates with the pristine structure. There is a suboxide binding energy in the scan as well, this is due to the argon etch of the film causing a reduction in the oxide creating what is seen as a suboxide in the spectra. Figure 2.8 (c) shows a high concentration of C-NH_2 bonds

within the film being much closer to that of the pristine MOF than the nonmodified PLD films. Figure 2.8 (d) the O1s peaks are precisely what would be expected for the film.

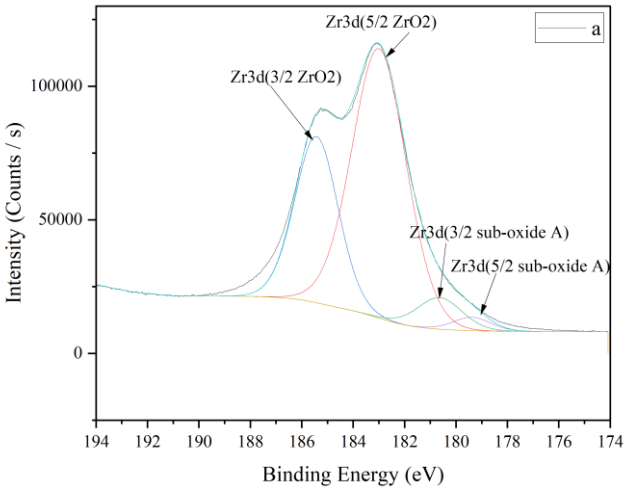

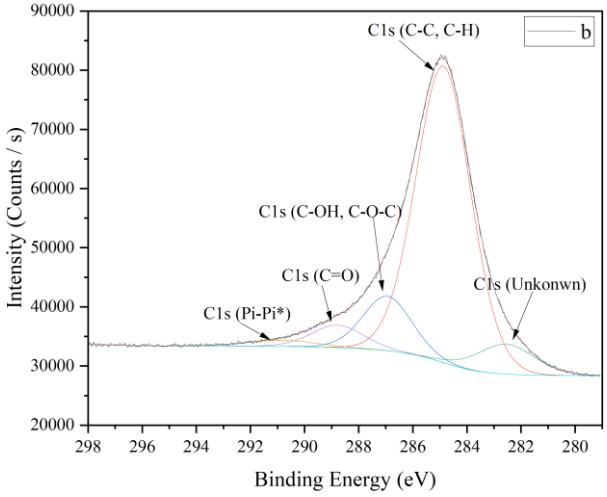

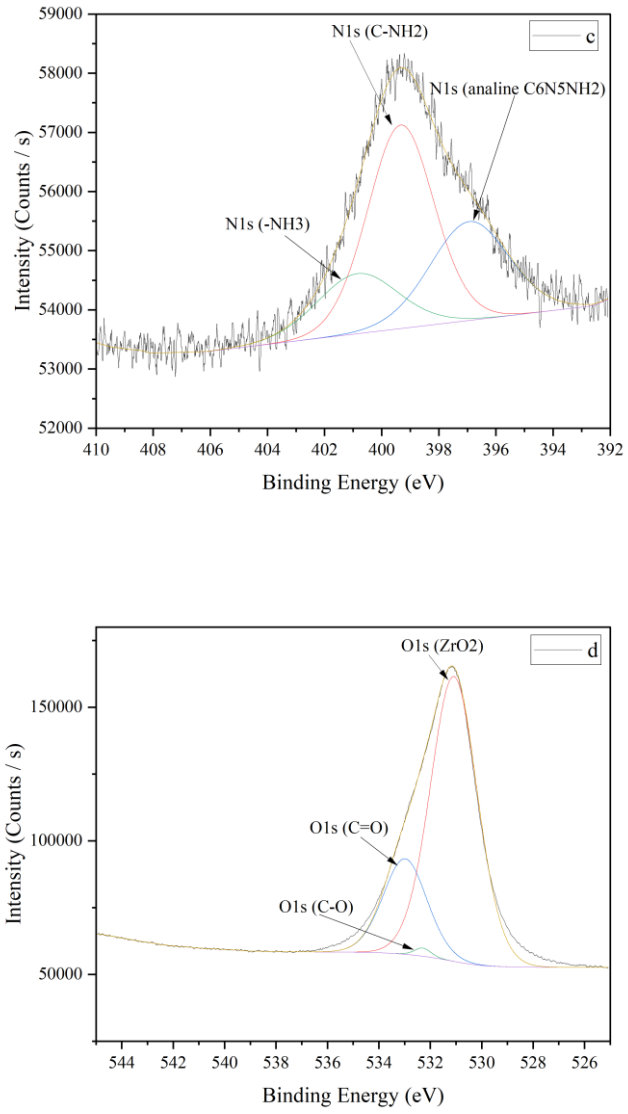

Figure 2.8: XPS high resolution Scan of modified UiO-66-NH_2 PLD film (a)Zr3d scan with deconvolution, (b) C1s scan with Deconvolution, (c) N1s scan with deconvolution, (d) O1s scan with deconvolution.

Table 4 contains the deconvoluted data from Figure 2.8. This table shows the deconvoluted peaks from the modified UIO-66-NH_2 film. This tabulated data shows the improvement made when compared to the unmodified data in table 3 showing that it is more like

that in the pristine MOF represented in table 2. This is a better representation of the suboxide to oxide ratio as well as the atomic compositions of each bond.

Table 4: XPS high resolution Scan of modified UiO-66-NH_2 PLD film deconvolution peaks tabulated.

Name	Peak BE	FWHM eV	Area (P) CPS.eV	Atomic %
Zr3d5/2 (Sub-oxide A)	179.38	1.74	9458	0.4
Zr3d3/2 (Sub-oxide A)	180.64	2.04	26174.45	1.6
Zr3d5/2 (ZrO2)	182.99	2.49	271847.03	11.48
Zr3d3/2 (ZrO2)	185.43	1.98	133783.11	8.21
C1s Scan C	282.55	2.48	13502.95	3.24
C1s (C-C,C-H))	284.87	2.39	129509.72	31.15
C1s (C-OH, C-O-C)	286.95	2.13	21200.63	5.11
C1s (C=O)	288.78	2.27	9325.76	2.25
C1s Pi-Pi*	290.81	3	3372.37	0.81
N1s (aniline C6H5NH2)	396.93	3.25	5885.87	0.91
N1s (C-NH2)	399.33	2.73	10198.71	1.58
N1s (-NH3)	400.85	3.36	3703.92	0.57
O1s (ZrO2)	531.08	2.15	248391.76	24.7
O1s (C-O)	532.29	0.77	2526.26	0.25
O1s (C=O)	532.98	2	77648.69	7.73

Figure 2.9 contains Raman spectroscopy for the PLD grown MOFs, with measurements performed on the Nexas G2 Surface analysis system. This is an ultra-high vacuum using a 532nm excitation laser. 0.1mW of power was supplied to the laser to not burn the sample. The collection exposure time was 20 seconds, with a pre-exposure time of 3 seconds. There were 50 sample exposures with no shift and a medium cosmic ray threshold to eliminate anomalies. The powder film under these conditions fluoresces to a point where the signal is only saturation, even

with attempts using fluorescence subtraction, baseline subtraction, etc. That same feature can be seen in the PLD films such that there is a saturation in the signal due to the fluorescence. In accordance with literature [23] the Raman signals at about 1600 and 1450 are from UIO-66-NH2. The same literature shows that the signal from the amine group changes the response in a way that makes the signal difficult to interpret. The COO peaks the two that appear in the spectra corelates with literature.

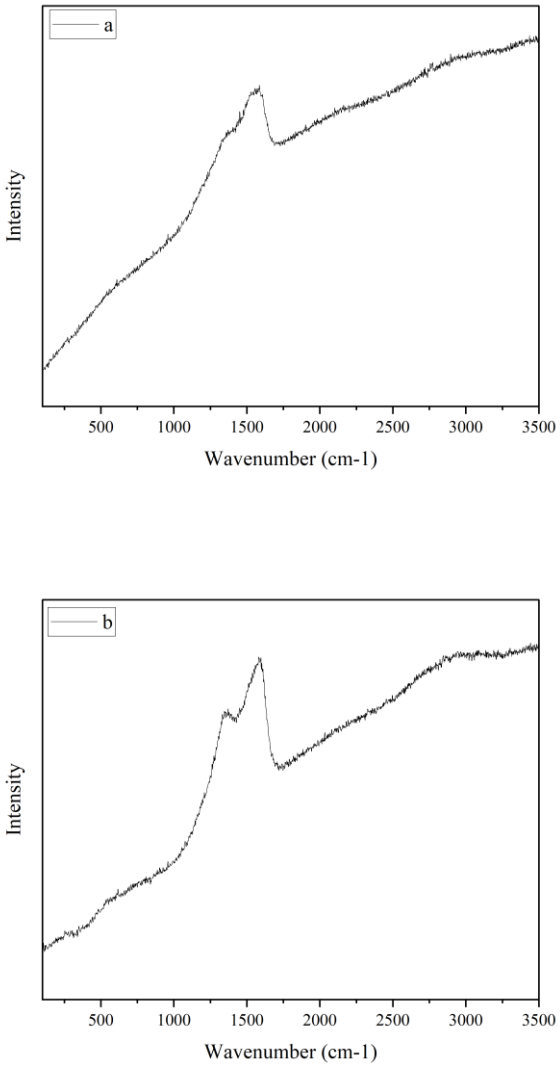

Figure 2.9: Raman spectroscopy for PLD Grown films, (a) UiO-66-NH_2 modified film Raman signal, (b) UiO-66-NH_2 PLD film Raman.

Figure 2.10 (a-d) contains Fourier Transform Infrared Spectroscopy performed with a Thermo Scientific Nicolet iS50 FT-IR; all samples were run using the iS50 ATR. This ATR is fitted with a diamond crystal on a dual source system, containing the Polaris^{TM} long-life IR source and a Tungsten-Halogen white light source. 32 scans were taken with a resolution of 4 at a data spacing of 0.482cm^{-1}. Backgrounds scans were taken prior to every sample with the diamond surface thoroughly cleaned, that background scan was subtracted from the measured spectrum automatically. PLD samples were grown onto gold as the absorption when grown on other substrates proved to be an issue, the high reflectance of the gold greatly improved the signal. Figure 2.10 (a), UiO-66-NH_2 pristine, matches closely with literature [24,25]. The starting material structure is critical for the self-assembly of the nucleation and growth process for the PLD of the MOF. Figure 2.10 (b) contains the spectra for 2-aminoterephthalic acid as to have a comparison for the additive in the modified PLD target. The UiO-66-NH_2 PLD grown shown in Figure 2.10 (c) to be highly promising that the MOF can survive and nucleate onto a gold substrate while maintaining the prober structure, which is not shown in XRD. The signal for Figure 2.10 (c) does not have the highest absorption. This makes sense due to the potentially porous structure, with little thickness having minimal material to absorb the light emitted by the instrument. With that said gold was the only substrate proven to have any significant IR response that wasn't overshadowed by the substrates, likely true for many metals. Figure 2.10 (d) proves that the modified target is the more efficient method of getting the desired chemical structure or bonds from the target to the substrate. Where the absorption for Figure 2.10 (c) and Figure 2.10 (d) are similar in scale there is a clear difference between the peak resolution and amplitude proving the modified method to be superior.

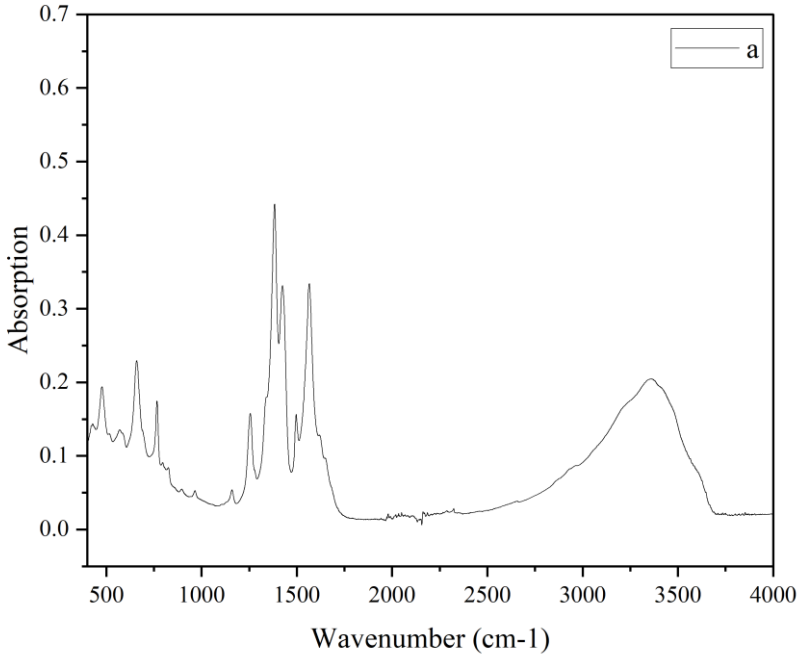
a
Absorption
0.0
0.1
0.2
0.3
0.4
0.5
0.6
0.7
500
1000
1500
2000
2500
3000
3500
4000
Wavenumber (cm-1)

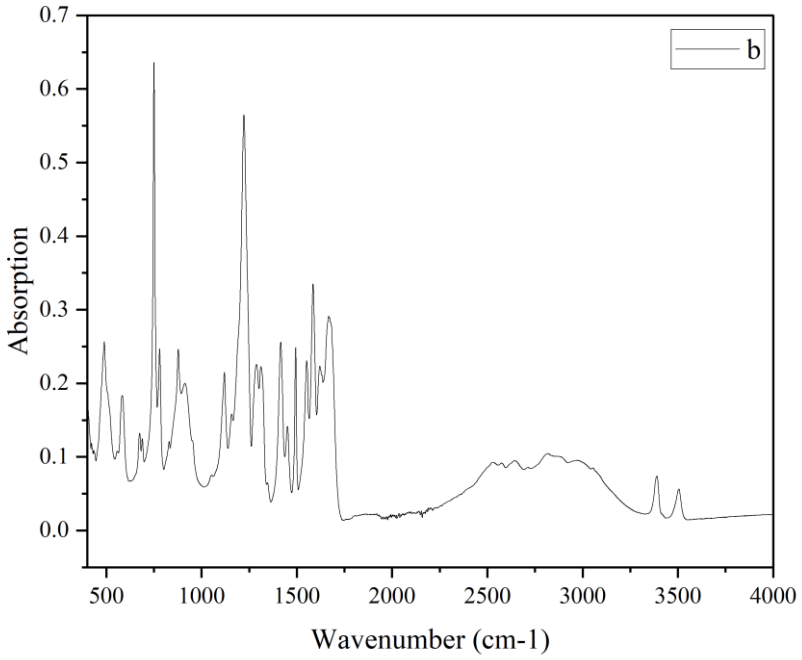
b
Absorption
0.0
0.1
0.2
0.3
0.4
0.5
0.6
0.7
500
1000
1500
2000
2500
3000
3500
4000
Wavenumber (cm-1)

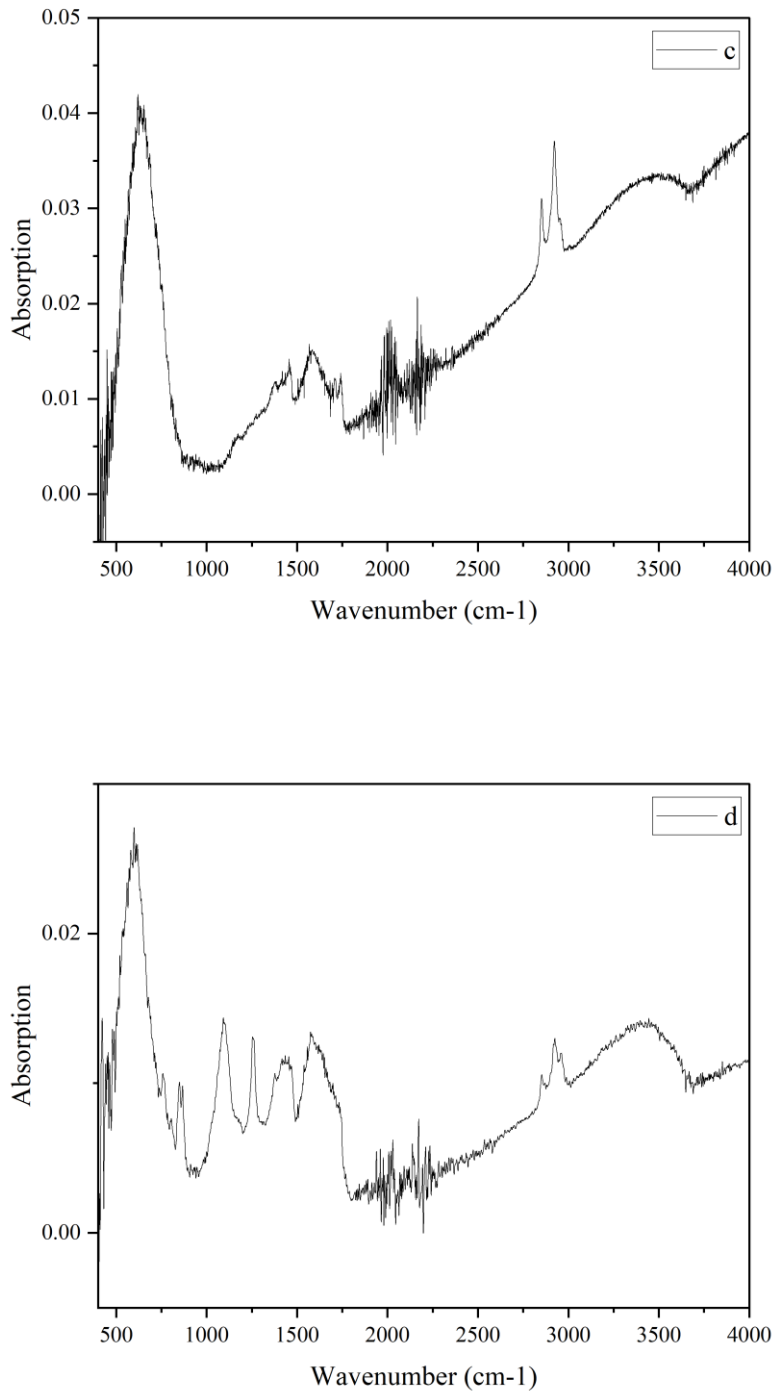

Figure 2.10: IR spectroscopy of samples, (a) Pristine UiO-66-NH_2, (b) 2-Aminoterephthalic acid, (c) UiO-66-NH_2 PLD on Au/SiO_2, (d) UiO-66-NH_2 Modified on Au/SiO_2

Film thickness was measured with a LEXT 3-D measuring laser microscope OLS5000 (LSCM). The 20x microscope lens was used to give a long working distance while still maintaining high performance. A laser source of 1mW max power and a wavelength of 400-420nm. The working distance allows for a large area of the film to be measured in a single scan without the need for stitching. This methodology has been cross checked with other samples using cross sectional SEM. A step height method was used to measure thicknesses in table 5, simply showing the thickness of the film on the substrate. This shows that the method for growth is consistent across 2 different runs for both is consistent, with that said there is some inherent film thickness error in the placement of the substrate in relation to the plume generated by the ablation of the target. This is due to not having a rotating substrate holder allowing for more uniform coverage of the substrate. The film grown with the modified target proves to be thicker when ablated at the same energy density and total shot count. Films were also grown on Al_2O_3 but proved to be impossible to interpret due to the extreme surface roughness of the substrate at +-1 um which would be in the order of 5x the thickness of the film, thus polished Silicon and silicon with a thermal oxide were used for the substrates.

Table 6 contains LSCM roughness values for PLD grown films. The root mean squared value (Sq) gives the standard deviation of the heights, effectively giving the value for the surface roughness itself. For these samples there are many things that contribute to the roughness of the film. Although the SiO_2 film would be nearly atomically smooth the sputtered film on top of it would give roughness as is known for all physical vapor deposition (PVD) methods. PLD being a PVD method itself is known to have relatively high surface roughness for samples, generally combated with high substrate temperature increasing mobility of atoms but this approach will not work for these samples. The nonmodified method would appear to have less roughness than the

modified method. A likely contributor to this is that the deposition rate is approximately 21% less, calculated by ratio of film thickness. Slower deposition rates generally produce a smoother film, this could be solved by increasing the delay between laser pulses. Such a delay was tested to generate less heat on the target itself causing less carbonization of the target material.

Table 5: LSCM of PLD grown films for thickness in nanometers.

Sample	Film Thickness (nm)
UIO-66-NH2 100C Si	173
UIO-66-NH2 100C SiO2-Au	170
UIO-66-NH2 100C Modified 1	210
UIO-66-NH2 100C Modified 2	225

Table 6: LSCM of PLD grown films for film roughness investigation in nanometers.

Sample	Sq [nm]	Ssk	Sku	Sp [nm]	Sv [nm]	Sz [nm]	Sa [nm]	Sdq	Sdr [%]
UIO PLD 100C-2 Si	17	-0.099	4.577	245	475	720	13	0.041	0.08
UIO PLD 100C-2 SiO2-Au	8	-0.189	28.938	356	289	646	6	0.028	0.038
UIO-Modified PLD 100C 1	12	0.597	93.916	507	349	856	9	0.057	0.154
UIO-Modified PLD 100C 2	14	0.411	46.881	379	426	805	10	0.066	0.204

A 4-point probe was used to measure resistance with a Keithley 2700 multimeter, using a 4-wire resistance method. UiO-66-NH_2 grown on silicon measured to 3.4GΩ. UiO-66-NH_2 on Al_2O_3 measured to 10.1GΩ. The modified UiO-66-NH_2 on SiO_2 measured the same as if you

were to measure air showing that it is extremely resistive. This method could only be used on insulating substrates as conductive substrates would shorten the film and the measurement was the same as a bare substrate. This resistance being so high suggests that the bandgap of the grown film is high similar to that of the hydrothermally synthesized MOF.

In Table 7, dielectric measurements were made for PLD grown films to further explore their electrical properties. Using an Agilent 4294A LCR meter/probe station set up, measuring Cp-Cd, with a scan range of 100Hz to 10MHz. Selecting 100kHz for the analysis frequency, which is commonly used. A parallel plate method was used by using a conductive substrate and a gold top electrode of 1.75mm in diameter, deposited by sputtering gold with a stainless-steel mask. Using the equation below to calculate the dielectric constant.

$$\varepsilon r \left(\frac{F}{m}\right) = \frac{Film\ thickness\ \times Capacitance}{Electrode\ area\ \times Permittivity\ Constant} \quad (2.1)$$

For MOFs many things can affect the dielectric constant, such as pore size and distribution, film thickness, and even the MOF selected. The modified film shows the best dielectric constant of the samples. The UIO-66-NH_2 on Al_2O_3-au film thickness was assumed based on that grown on SiO_2-au. Overall samples prove to have lower dielectric constants thus a lesser ability to hold charge. This could entail a less likely application in energy storage but very promising for other applications. Having a highly resistive film with a low dielectric constant suggests that there is internal porosity which would confirm the MOF structure.

Table 7: Dielectric measurements for PLD grown films.

	Measured Capacitance (F)	Dissipation Factor (D)	Electrode Diameter (m)	Electrode Area (m^2)	Permittivity Constant (F/m)	Dielectric Constant (F/m)
UIO66-NH2 PLD Al2O3-Au	4.83E-13	2.87E-03	1.75E-03	2.41E-06	8.85E-12	3.86E-03
UIO66-NH2 Si PLD	1.07E-10	1.32E+00	1.75E-03	2.41E-06	8.85E-12	8.73E-01
UIO66-NH2 PLD SiO2-Au	5.68E-13	3.80E-02	1.75E-03	2.41E-06	8.85E-12	4.53E-03
UIO66-NH2 PLD SiO2-Au 2	5.78E-13	1.55E-02	1.75E-03	2.41E-06	8.85E-12	4.70E-03
UIO66-NH2 PLD Modified	2.14E-10	2.64E-02	1.75E-03	2.41E-06	8.85E-12	2.11E+00
UIO66-NH2 100CModified-2	6.03E-13	3.77E-02	1.75E-03	2.41E-06	8.85E-12	6.37E-03

Conclusion

This research shows a very strong attempt at growing a thin film MOF of UiO-66-NH_2 with some exploration into electrical properties. This PLD approach, although difficult, is promising for future device applications for MOFs. XPS and FTIR analysis prove to have promising results for the characterization of the film. XRD and Raman done on the films prove to be difficult methods to analyze the films. Electrical measurements show to be insulating with little ability to hold charge. Not only does this research show that there is potential for the growth of a metal organic structure from a previous structure with the unmodified target, but it includes an improvement on that process with the modified method. With the evaluation of the XPS data a stoichiometric ratio of the additive structure to giving a more similar film. This similarity was explored and confirmed by both XPS and IR spectroscopy. IR spectroscopy shows that the modified method is potentially more like the pristine MOF, which directly correlates with the

XPS data. Film thickness and roughness was explored with a laser scanning confocal microscope showing that the modified target produced a thicker film, thus having a greater deposition rate potentially contributing to the improved electrical properties. The roughness for the modified samples was more than that of the unmodified. As this is exploratory there is room for a variety of experiments and tests to be done to improve the film quality and process.

References

[1] Stassen, I., B. Bueken, H. Reinsch, J. F. M. Oudenhoven, D. Wouters, J. Hajek, V. Van Speybroeck, et al. "Towards Metal–Organic Framework Based Field Effect Chemical Sensors: UiO-66-NH 2 for Nerve Agent Detection." Chemical Science 7, no. 9 (2016): 5827–32. https://doi.org/10.1039/C6SC00987E.

[2] Zhang, Qiangsheng, Xue Jiang, Alexander M. Kirillov, Yanwen Zhang, Mingyang Hu, Wei Liu, Lizi Yang, Ran Fang, and Weisheng Liu. "Covalent Construction of Sustainable Hybrid UiO-66-NH2@Tb-CP Material for Selective Removal of Dyes and Detection of Metal Ions." ACS Sustainable Chemistry & Engineering 7, no. 3 (February 4, 2019): 3203–12. https://doi.org/10.1021/acssuschemeng.8b05146.

[3] Zhai, Shaoxiong, Xiaoyang Jia, Zhongrui Lu, Yuna Ai, Xin Liu, Jun Lin, Shaojian He, Qian Wang, and Lin Chen. "Highly Ion Selective Composite Proton Exchange Membranes for Vanadium Redox Flow Batteries by the Incorporation of UiO-66-NH2 Threaded with Ion Conducting Polymers." Journal of Membrane Science 662 (October 15, 2022): 121003. https://doi.org/10.1016/j.memsci.2022.121003.

[4] Ranjith Kumar, Deivasigamani, Raj Karthik, Ganesh Dhakal, Van Quang Nguyen, Jintae Lee, and Jae-Jin Shim. "Catechol Redox Couple Functionalized Metal-Organic Framework UiO-66-NH2 as an Efficient Catalyst for Chromium Ion Sensor in Water Samples." Journal of Cleaner Production 374 (November 10, 2022): 133731. https://doi.org/10.1016/j.jclepro.2022.133731.

[5] Suriyakumar, Shruti, A. Manuel Stephan, N. Angulakshmi, Mohamed H. Hassan, and Mohamed H. Alkordi. "Metal–Organic framework@SiO2 as Permselective Separator for Lithium–Sulfur Batteries." Journal of Materials Chemistry A 6, no. 30 (July 31, 2018): 14623–32. https://doi.org/10.1039/C8TA02259C.

[6] Zhang, Qi, Sijia Wang, Ye Liu, Mengting Wang, Rentian Chen, Zongyuan Zhu, Xiangyun Qiu, Shoudong Xu, and Tao Wei. "UiO-66-NH2@67 Core–Shell Metal–Organic Framework as Fillers in Solid Composite Electrolytes for High-Performance All-Solid-State Lithium Metal Batteries." Energy Technology 11, no. 4 (2023): 2201438. https://doi.org/10.1002/ente.202201438.

[7] Jarai, Bader M., Zachary Stillman, Lucas Attia, Gerald E. Decker, Eric D. Bloch, and Catherine A. Fromen. "Evaluating UiO-66 Metal–Organic Framework Nanoparticles as Acid-Sensitive Carriers for Pulmonary Drug Delivery Applications." ACS Applied

Materials & Interfaces 12, no. 35 (September 2, 2020): 38989–4. https://doi.org/10.1021/acsami.0c10900.
[8] Redfern, Louis R., Lee Robison, Megan C. Wasson, Subhadip Goswami, Jiafei Lyu, Timur Islamoglu, Karena W. Chapman, and Omar K. Farha. “Porosity Dependence of Compression and Lattice Rigidity in Metal–Organic Framework Series.” Journal of the American Chemical Society 141, no. 10 (March 13, 2019): 4365–71. https://doi.org/10.1021/jacs.8b13009.
[9] Cai, Mengru, Gongsen Chen, Liuying Qin, Changhai Qu, Xiaoxv Dong, Jian Ni, and Xingbin Yin. “Metal Organic Frameworks as Drug Targeting Delivery Vehicles in the Treatment of Cancer.” Pharmaceutics 12, no. 3 (March 2020): 232. https://doi.org/10.3390/pharmaceutics12030232.
[10] Kandiah, Mathivathani, Merete Hellner Nilsen, Sandro Usseglio, Søren Jakobsen, Unni Olsbye, Mats Tilset, Cherif Larabi, Elsje Alessandra Quadrelli, Francesca Bonino, and Karl Petter Lillerud. “Synthesis and Stability of Tagged UiO-66 Zr-MOFs.” Chemistry of Materials 22, no. 24 (December 28, 2010): 6632–40. https://doi.org/10.1021/cm102601v.
[11] Bétard, Angélique, and Roland A. Fischer. “Metal–Organic Framework Thin Films: From Fundamentals to Applications.” Chemical Reviews 112, no. 2 (February 8, 2012): 1055–83. https://doi.org/10.1021/cr200167v.
[12] Shekhah, Osama, Hui Wang, Stefan Kowarik, Frank Schreiber, Michael Paulus, Metin Tolan, Christian Sternemann, et al. “Step-by-Step Route for the Synthesis of Metal−Organic Frameworks.” Journal of the American Chemical Society 129, no. 49 (December 1, 2007): 15118–19. https://doi.org/10.1021/ja076210u.
[13] Ariga, Katsuhiko. “Chemistry of Materials Nanoarchitectonics for Two-Dimensional Films: Langmuir–Blodgett, Layer-by-Layer Assembly, and Newcomers.” Chemistry of Materials 35, no. 14 (July 25, 2023): 5233–54. https://doi.org/10.1021/acs.chemmater.3c01291.
[14] Yoo, Yeonshick, and Hae-Kwon Jeong. “Heteroepitaxial Growth of Isoreticular Metal−Organic Frameworks and Their Hybrid Films.” Crystal Growth & Design 10, no. 3 (March 3, 2010): 1283–88. https://doi.org/10.1021/cg9013027.
[15] Hermes, Stephan, Felicitas Schröder, Rolf Chelmowski, Christof Wöll, and Roland A. Fischer. “Selective Nucleation and Growth of Metal−Organic Open Framework Thin Films on Patterned COOH/CF3-Terminated Self-Assembled Monolayers on Au(111).” Journal of the American Chemical Society 127, no. 40 (October 1, 2005): 13744–45. https://doi.org/10.1021/ja053523l.
[16] Kubo, Masaru, Watcharop Chaikittisilp, and Tatsuya Okubo. “Oriented Films of Porous Coordination Polymer Prepared by Repeated in Situ Crystallization.” Chemistry of Materials 20, no. 9 (May 1, 2008): 2887–89. https://doi.org/10.1021/cm800371b.
[17] Schoedel, Alexander, Camilla Scherb, and Thomas Bein. “Oriented Nanoscale Films of Metal–Organic Frameworks By Room-Temperature Gel-Layer Synthesis.” Angewandte Chemie 122, no. 40 (2010): 7383–86. https://doi.org/10.1002/ange.201001684.
[18] Mueller, U., M. Schubert, F. Teich, H. Puetter, K. Schierle-Arndt, and J. Pastré. “Metal–Organic Frameworks—Prospective Industrial Applications.” Journal of Materials Chemistry 16, no. 7 (February 3, 2006): 626–36. https://doi.org/10.1039/B511962F.
[19] Redfern, Louis R., Lee Robison, Megan C. Wasson, Subhadip Goswami, Jiafei Lyu, Timur Islamoglu, Karena W. Chapman, and Omar K. Farha. “Porosity Dependence of Compression and Lattice Rigidity in Metal–Organic Framework Series.” Journal of the

American Chemical Society 141, no. 10 (March 13, 2019): 4365–71. https://doi.org/10.1021/jacs.8b13009.

[20] Chrisey, D. B., A. Piqué, R. A. McGill, J. S. Horwitz, B. R. Ringeisen, D. M. Bubb, and P. K. Wu. “Laser Deposition of Polymer and Biomaterial Films.” Chemical Reviews 103, no. 2 (February 1, 2003): 553–76. https://doi.org/10.1021/cr010428w.

[21] Krebs, Hans-Ulrich, Martin Weisheit, Jörg Faupel, Erik Süske, Thorsten Scharf, Christian Fuhse, Michael Störmer, et al. “Pulsed Laser Deposition (PLD) -- A Versatile Thin Film Technique.” In Advances in Solid State Physics, edited by Bernhard Kramer, 505–18. Advances in Solid State Physics. Berlin, Heidelberg: Springer, 2003. https://doi.org/10.1007/978-3-540-44838-9_36.

[22] Connolly, B. M., M. Aragones-Anglada, J. Gandara-Loe, N. A. Danaf, D. C. Lamb, J. P. Mehta, D. Vulpe, et al. “Tuning Porosity in Macroscopic Monolithic Metal-Organic Frameworks for Exceptional Natural Gas Storage.” Nature Communications 10, no. 1 (May 28, 2019): 2345. https://doi.org/10.1038/s41467-019-10185-1.

[23] Timofeev, Konstantin L., Sergei A. Kulinich, and Tamara S. Kharlamova. “NH2-Modified UiO-66: Structural Characteristics and Functional Properties.” Molecules 28, no. 9 (May 5, 2023): 3916. https://doi.org/10.3390/molecules28093916.

[24] Luu, Cam Loc, Thi Thuy Van Nguyen, Tri Nguyen, and Tien Cuong Hoang. “Synthesis, Characterization and Adsorption Ability of UiO-66-NH2.” Advances in Natural Sciences: Nanoscience and Nanotechnology 6, no. 2 (February 2015): 025004. https://doi.org/10.1088/2043-6262/6/2/025004.

[25] Abid, Hussein Rasool, Jin Shang, Ha-Ming Ang, and Shaobin Wang. “Amino-Functionalized Zr-MOF Nanoparticles for Adsorption of CO2 and CH4.” International Journal of Smart and Nano Materials 4, no. 1 (March 1, 2013): 72–82. https://doi.org/10.1080/19475411.2012.688773.

Chapter 3: Thin film UiO66-NH2 MOF for the Detection of Heavy Metals in Water

Abstract

A thinfilm approach to UiO-66-NH_2 being used in the phiseoadsorption of heavy metal ions for detection in water. Pulsed laser deposition method was used to grow MOF thin-films on a gold working electrode. Working electrodes were manufactured with a titanium adhesion layer and gold as the electrode. Electrodes analyzed with laser scanning confocal microscope (LSCM), Fourier transform infared spectroscopy (FTIR) square wave stripping voltometry (SWSV), cylic voltametry (CV).

Experimental Method

Chapter 2 entails two different approaches for the manufacture of a MOF thin-film, the modified approach was used as it most closely forms a structure similar to the UiO-66-NH_2 which literature shows to have electrochemcial detection of heavy metals, detailed below. Much of the backgound information for this MOF was covered in chapter 2. Some additional resources were used for the chemical sensing application of the mof in this work [1-7].

Working electrodes were created on Al_2O_3 and Si/SiO_2 with a thermal oxide of 500nm. Titanium sputtered as an adhesion layer onto both substrates using a mask electrode, film thickness was checked with ellipsometry where polished silicon was used as a control sample. Gold was then sputtered onto the same substrates with no adjustments made to the mask. Gold and titanium were sputtered on a Semicore Sputtering system. The titanium target was from Kurt J. Lesker and 99.995% purity. The gold target was also ordered from Kurt J. Lesker with a purity of 99.999%. Titanium sputtered using radio frequency sputtering. A base vacuum of 1.5×10^{-5}

Torr was achieved, with a deposition pressure of 2.5×10^{-3} Torr. At a power of 100W and measured with ellipsometry for the desired thickness. For the deposition of gold, the same base vacuum was reached. With a deposition pressure of 2.0×10^{-3} with an ignition pressure of 2.5×10^{-2}. A power of 50W was used to get the desired 100nm thickness, resistance was checked to ensure that the film was conductive.

Pulsed laser deposition was done with a substrate temperature of 100℃, in an inert environment of Argon at a pressure of 0.001 mbar, followed a base vacuum of approximately 1×10^{-6} mbar. These parameters were used for all substrates, as well as both the pristine and modified targets. A solid state Quantel ND: YAG laser with a 266nm wavelength, thus emitting photons in the fourth harmonic. A 10Hz repetition rate with a pulse width of 150μs and a FL-Q switch Delay of 140μs, giving a 1.2mW pulse with an area of 0.2236 cm^2. The substrate was placed on the substrate holder 30mm from the surface of the target. For this set up the incident beam is focused on the target with an angle of 60º normal to the surface. 15,000 shots were used to grow the film with an additional 500 shots to remove any contamination from the surface of the target. Prior to deposition all substrates were thoroughly cleaned with methanol and deionized water, with sonication in methanol and rinsing with deionized water.

UiO-66-NH2 has been used to detect heavy metals in water. UiO-66-NH_2 PANI composite has been used to achieve a detection of $0.5\mu gL^{-1}$ of cadmium in water [1]. Developmental work on UiO-66-NH_2 shows the charge dependent uptake of contaminants [2]. The use of UiO-66-NH_2 for the adsorption of heavy metals such as Cd^{2+}, Cr^{3+}, Pb^{2+}, and Hg^{2+} has been shown to have high efficiency in the removal from water [3]. This methodology directly relates to the approach in using it for detection in this work. Grown electrodes were tested with cylic voltametry (CV) prior to square wave stripping voltametry (SWSV). A three electrode

system was used, the fabricated working electrode, a platnium wire counter electrode and a reference electrode of Ag/AgCl ordered from Base. The reference electrode was in a solution of 3M KCl.

Working solutions were in 0.1M KNO3 and 0.1M Potassium Acetate, both purchased from sigma aldridch, both with 99% purity. The analyte of choice for this work was lead, in the form of lead nitrate 99% purity purchased from sigma aldridch. Lead working solutions ranged from $0.1\mu gL^{-1}$ to $500\mu gL^{-1}$ for these solutions a PH of 5 was used, to achieve PH 5 nitric acid was used in all solutions. SWSV measurements were done two ways, for gold and for PLD MOF coated electrodes. For the gold, there was an initial voltage of -1 V and a final voltage of 0.1 V. The step size for scans was 2 mV, with a frequesncy of 25 Hz, and a pulse size of 25 mV. The electrode area being defined by the 2mm diameter of the sputtered electrode. There was an accumulation time of 180 seconds and an equilibration time of 30 seconds. The SWSV for the MOF film was different due to the adsorbitive nature of the film. Films were stirrred in a lead solution for 24 hours at 500 rmp with a magnetic stirrer. Magnetic stirring for the adsorption allows for more repeatable results, if solutions are not stirred it is a function of random vibration within the lab [8]. SWSV of these filims was done with a 30 second accumulation time and a 30 second equilibration time. A Gamry Instruments Interface 1010E was used for all electrochemical measurements.

CV scans were performed in 1mmol of $Fe(CN)_6$, dissolved from potassium hexacyanoferrate (III) 99% purity from sigma aldrich. CV Scans were taken with an initial voltage of 0 V and a limit of 0.5 V with a lower limit of -0.5V, the final voltage was 0V. There was a scan rate of 100mV/s with a step size of 5mV. The electrode area was defined by the

geometry of the sputtered electrode, with electrodes being 2mm in diameter. This method correlates with reproducable methods proven by literature [9].

Results and Discussion

The titanium adhesion layer was measured with a J.A. Woollam M-2000 Ellipsometer. Wavlengths from 193 to 1700nm were measured. Measurements taken at four angles from 60 to 75 in increments of five degrees. This measurement shows the film thickness to be 8.86nm showin in Figure 3.1 (a), this is follows literature which shows a minimum thickness of 2nm [10]. That same publication goes on to discuss the effect of a thicker titanium adhesion layer on the polarization fo the film as well as ressonance of the film, which was studied with ellipsometry. Figure 3.1 (b) is the optical model for fitting the psi and delta curves from the measurement. Si_JAW is simply the silicon substrate that is polished cauchy is the distribution that best fit the data. The MSE shown in figure 3.1 (a) at 7.876 is an acceptable fit, with 1 being an identical fit. Figure 3.1 (c) is a visual of the fitted curves overlayed with the fit curve. Having a proper fit in the lower wavelength insures the accuracy of the thickness measurement for ultra-thin films. Ellipsometry was also done on the pld grown films, innitialy seeming to have a great success but the cross comparison with another measurement proved that there was an issue. With an error of 2x on the film thickness and measurements not being able to get a good MSE suggesting quality fit the antisotropy was used to try the fit, It proved more successful. Without a deffinite way to determine the antisotropy and its effect on this measurement the data was not used for MOF film measurements.

(a)

Fit Results

MSE = 7.876
Thickness # 1 = 8.86 ± 0.014 nm
A = 2.344 ± 0.006774
B = -0.01921 ± 0.001579
C = -0.00014304 ± 5.7848E-05
k Amplitude = 0.72626 ± 0.003254
Exponent = 0.00775 ± 0.002138

(b)

Layer # 1 = Cauchy Thickness # 1 = 8.86 nm (fit)
A = 2.344 (fit) B = -0.01921 (fit) C = -0.00014304 (fit)
Urbach Absorption Parameters
k Amplitude = 0.72626 (fit) Exponent = 0.00775 (fit)
Band Edge = 400.0 nm
Substrate = Si_JAW

(c)

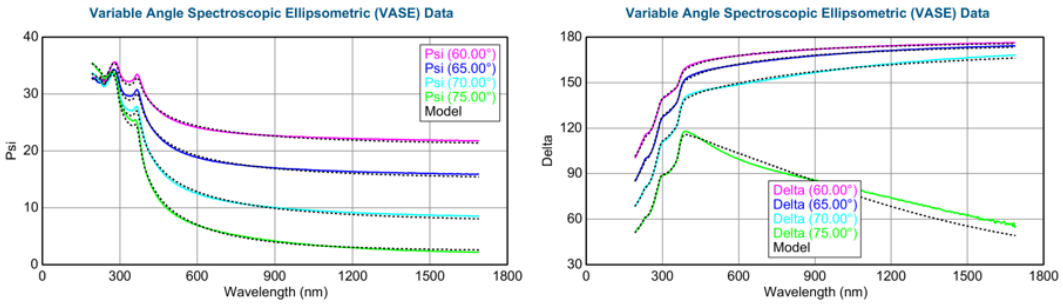

Figure 3.1: Film thickness measurement of Ti adhesion layer using ellipsometry, (a) being the fit results, (b) is the optical model used to fit the scan data, (c) contains the scan data and the fitted curve for both Psi and Delta.

Laser scanning confocal microscopy (LSCM) was used to analyze both sputtered gold films as well as UiO-66-NH2 PLD film on the electrode. Using a LEXT 3-D measuring laser microscope OLS5000 (LSCM). Fitted with a 20x microscope lens was used to give a long working distance while still maintaining high performance. A laser source of 1mW max power and a wavelength of 405nm. Table 8 shows A film thickness of 114nm on SiO_2 but 1817nm on Al_2O_3, this is entirely due to the extreme roughness on the alumina surface. High surface roughness is a positive for electrochemical applications but at the expense of measurability of the film. When accounting for the approximate 114 is within error for the measurement having a goal of 100nm thickness of gold, is 109 with the adhesion layer added.

Table 8: LSCM Measurements for film thickness and surface roughness, containing data for both sputtered electrodes and PLD grown film on the electrode.

Sample	Sq [nm]	Ssk	Sku	Sp [nm]	Sv [nm]	Sz [nm]	Sa [nm]	Sdq	Sdr [%]	Film Thickness (nm)
Au electrode SiO2 3	72	-0.953	5.725	765	1263	2028	52	37	0.092	114
Au electrode Al2O3	1243	-0.289	6.371	13040	13145	26185	920	1149	52.747	1817
Au electrode SiO2 Modified UIO66-NH2 PLD	58	23.243	882.853	2662	1134	3796	28	56	0.15	446
Au electrode SiO2 Modified UIO66-NH2 PLD S2	20	-4.653	212.911	465	832	1297	14	36	0.08	502

Figure 3.2 (a) shows the Ti/Au working electrode deposited onto a Si/SiO_2 substrate. Figure 3.2 (b) shows the deposition of the same working electrode mask onto Al_2O_3 substrate. Substrates were then cut with a LPKF ProtoLaser S4 into individual devices, using a 532nm laser with percise cutting. Electrodes have to be cut into devices prior to the film deposition due to the differences in the coverage are of the two PVD systems. Figure 3.2 (c), a kapton mask was used to protect the electrode. Kapton tape and kapton substrate were both attempted, with kapton substrate proving to be a more robust method. This does come price in the shadow effect of the thicker film, effectively giving a lower thickness off of the ti/au electrode than on. Masks were oversized to insure full coverage of the electrode. Figure 3.2 (d) Shows a coplete electrode with the PLD grown UiO-66-NH_2 film. Kapton tape was used to form an insulating barrior overe the

ti/au electrode to not short the film. Copper tape was added to the connection point of the electrode due to the clipping rubbing away the 100nm ti/au film.

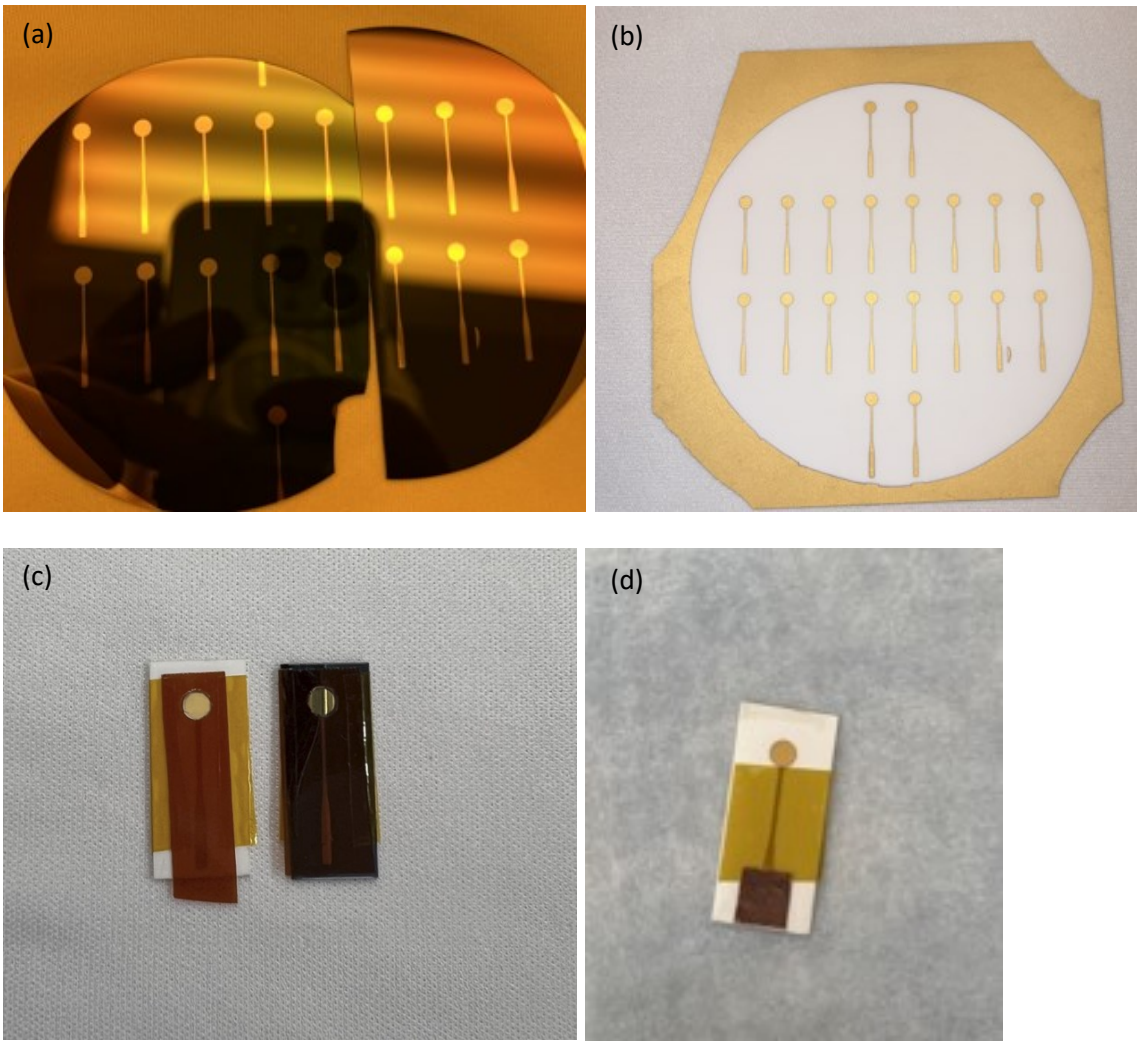

Figure 3.2: Created Working electrodes at various stages in the manufacturing process, on both silicone dioxide and alumina, (a) Sputtered gold electrodes on SiO_2, (b) Sputtered gold electrodes on Al_2O_3, (c) Masked working electrodes for PLD of UiO-66-NH_2 film, (d) final prepped film for the use as an electrochemical sensor.

LSCM imaging of the physical vapor deposited electrode shown in figure 3.3. Figure 3.3 (a,b) show visual images of the height of the film. Figure 3.3 (b) is the scan of the film shown as height of the film. Figure 3.3 (c) shows the profile across the electrode. The PLD film was done

such that the area of the pld was larger than the gold as to not short the MOF film. This would ensure an honest test of the PLD UiO-66-NH_2 raher than the gold. That is also the reason that gold was chosen as the electrochemical potential of gold to lead is different than that of carbon to lead that UiO-66-NH_2 would show.

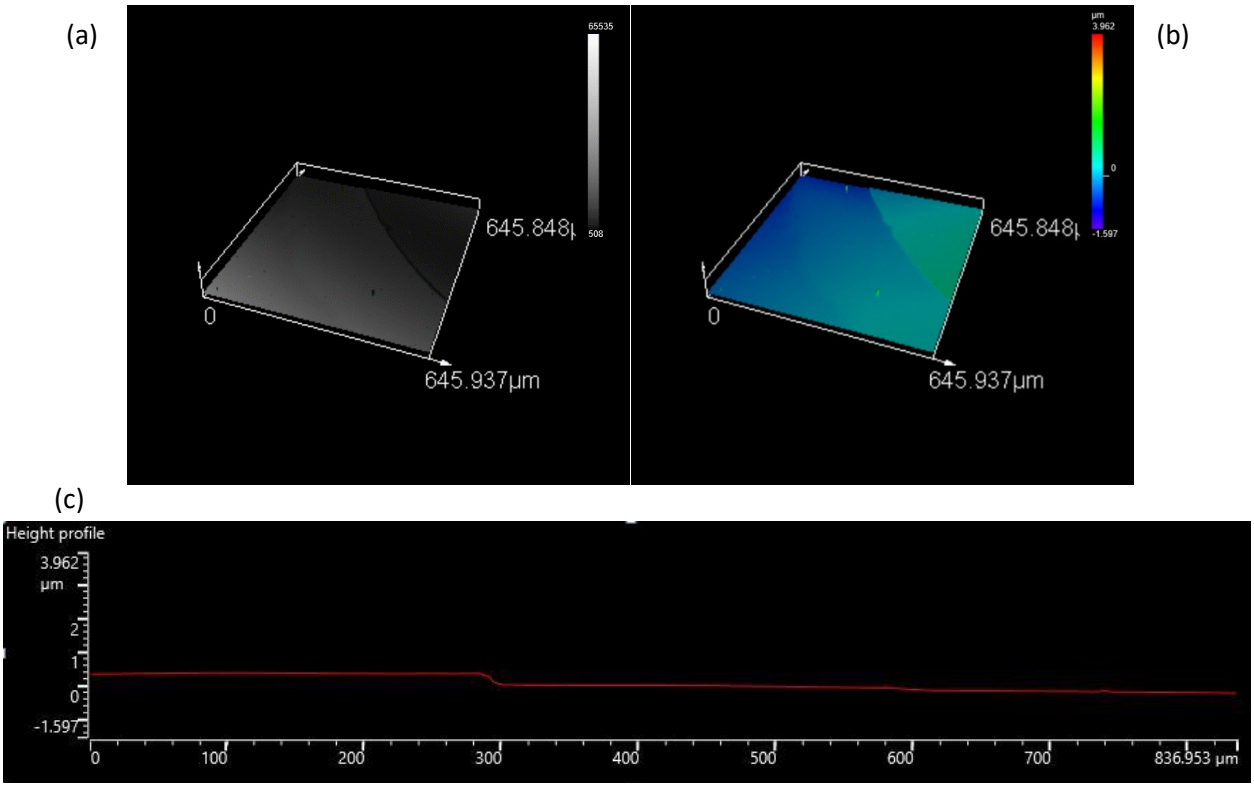

Figure 3.3 LSCM of the PLD UiO-66-NH_2 film on the Au electrode on SiO_2 substrate, (a) A black and white image of the scanned electrode. (b) a height scan of the film, (c) Profile in a line of the scanned electrode

The PLD grown UiO-66-NH_2 film was confirmed with IR spectroscopy. Fourier Transform Infrared Spectroscopy (FTIR) was performed with a Thermo Scientific Nicolet iS50 FT-IR; run using the iS50 ATR. This ATR is fitted with a diamond crystal on a dual source system, containing the PolarisTM long-life IR source and a Tungsten-Halogen white light source. 32 scans were taken with a resolution of 4 at a data spacing of 0.482cm-1. Backgrounds

scans were taken prior to every sample with the diamond surface thoroughly cleaned, background scans were automatically subtracted after the sample measurement. Figure 3.4 shows the IR spectroscopy of the UiO-66-NH_2 PLD grown on the gold working electrode. This matches closely with the Modified UiO-66-NH_2 from chapter 2, Figure 2.10. Also in that same figure there is the pristine and the additive, this data is in line with those as well.

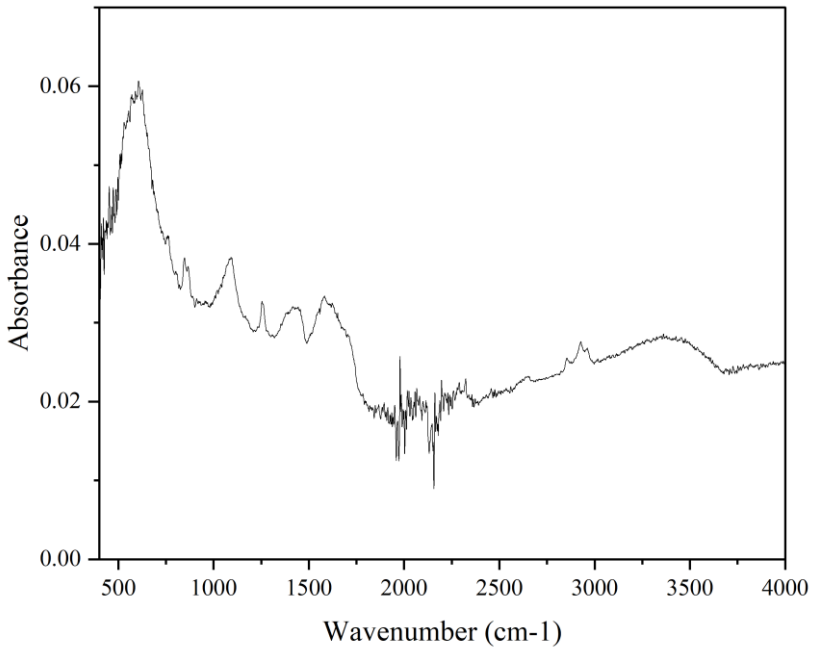

Figure 3.4: IR spectroscopy of UiO-66-NH_2 on the sputtered gold working electrode, the substrate for this sample was SiO_2.

Cyclic voltammetry is a technique used to show the oxidation and reduction reaction of an electrode. $[Fe(CN)_6]^{3-/4-}$ is commonly used to study electrodes in their development due to its nearly reversible redox reaction [10]. Figure 3.5 (a) shows 6 consecutive CV scans of $Fe(CN)_6$ using the Ti/Au electrode on the alumina substrate. These scanns are supported by what you

would expect according to literature [10]. Figure 3.5 (b) shows the Ti/Au electrode on Si/SiO_2 measured with 5 CV scans in the $Fe(CN)_6$ solution. These scans show that there is an issue with this configuration, and many attempts were made to accoplish this. The comparison between these two scans shows why alumina was choosen as the electrochemical substrate of choice for this work. Figure 3.5 (c) show 5 consecutive CV scans of the buffer solution, 0.1M KNO_3 and 0.1M Potassium Acetate at a PH of 5 which was achieved with addition of nitric acid. Figure 3.5 (d) shows 6 consecutive CV scans of the PLD deposited UiO-66-NH_2 on the Ti/Au working electrode with a Al_2O_3 substrate. These scans show a change in the direction of the bare electrode, which would suggest a delamination of the electrode or an exceptional film has been produced. It would turn out that upon further examination the film delaminates from the gold due to lack of adhesion. Literature shows that there are resuable approachs to the extraction and remediation for the removal of gold from water using UiO-66-NH_2 [11-13]. This would suggest that the adhesion mechanisms for the MOF to gold are such that it is not strongly bound, which makes perfect sense. In the case of gold that is common for the adhesion of most compounds to the surface, therefore the film is likely delaminating from the surface of the gold. Producing scans that would seem to be similar to the gold, because they are from the underlying gold electrode shorting the MOF film through holes in the film and delamination points. The only way to overcome this would be with the change of the electrode. With that being said this does show a possibility of the film being used for gold remediation in solutions as it accumulates due to the electronegativity of the film rathat than the electrochemical potential applied.

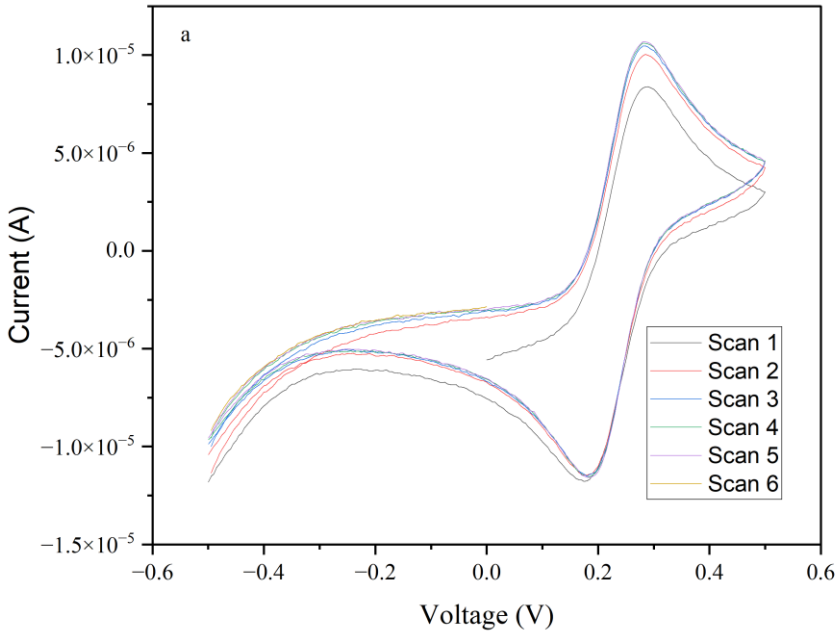
a
1.0×10⁻⁵
5.0×10⁻⁶
0.0
−5.0×10⁻⁶
−1.0×10⁻⁵
−1.5×10⁻⁵
Current (A)
−0.6
−0.4
−0.2
0.0
0.2
0.4
0.6
Voltage (V)
Scan 1
Scan 2
Scan 3
Scan 4
Scan 5
Scan 6

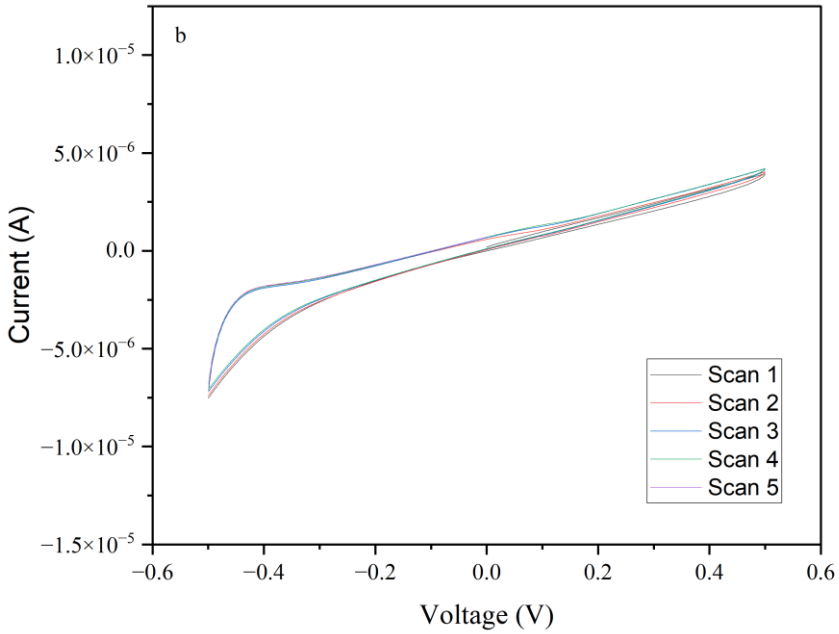
b
1.0×10⁻⁵
5.0×10⁻⁶
0.0
−5.0×10⁻⁶
−1.0×10⁻⁵
−1.5×10⁻⁵
Current (A)
−0.6
−0.4
−0.2
0.0
0.2
0.4
0.6
Voltage (V)
Scan 1
Scan 2
Scan 3
Scan 4
Scan 5

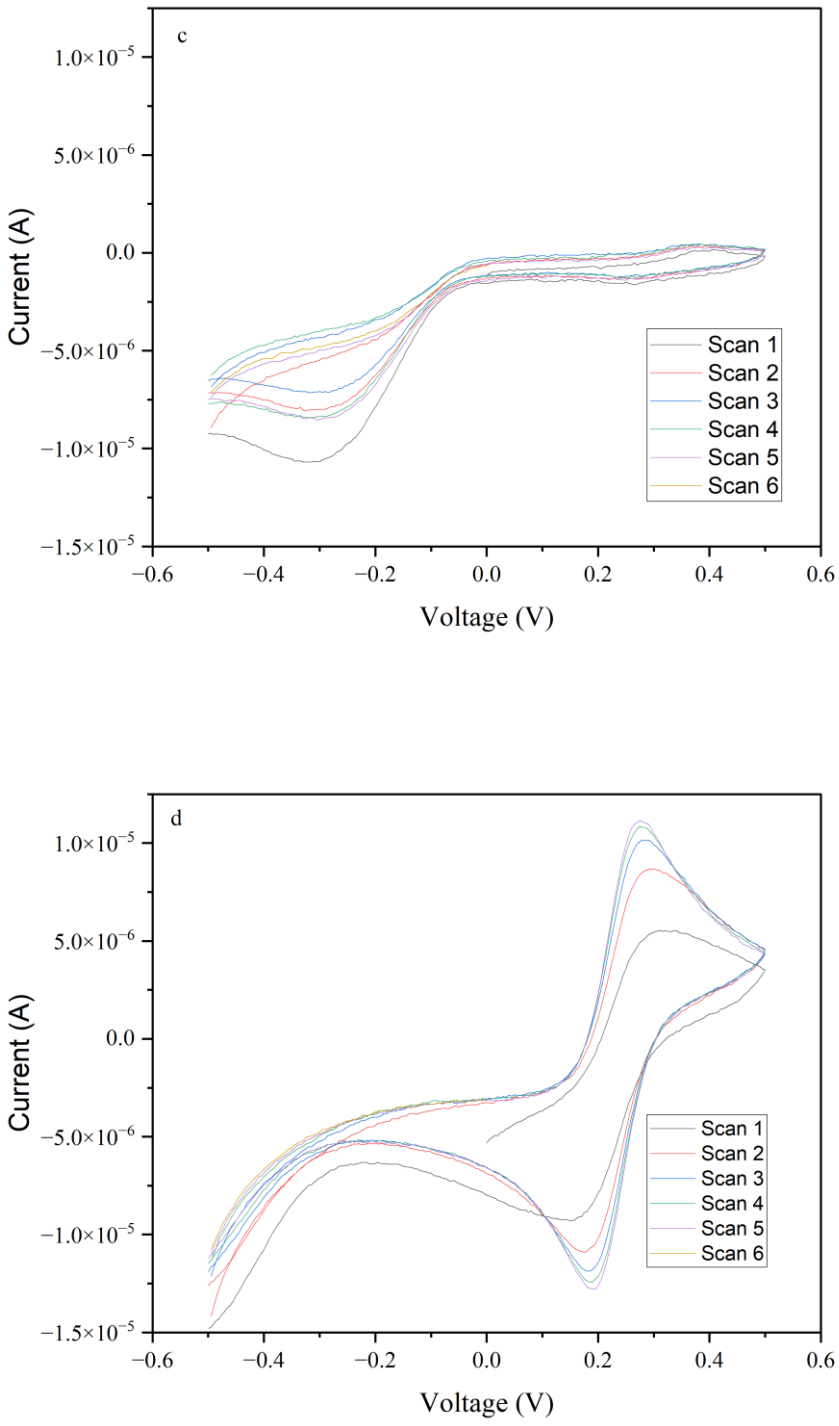

Figure 3.5: Cyclic Voltammetry scans of various electrodes in $Fe(CN)_6$ and buffer, (a) CV scan of Ti/Au bare electrode on Al_2O_3 in $Fe(CN)_6$, (b) CV scan of Ti/Au bare electrode on SiO_2 in $Fe(CN)_6$, (c) CV scan of Ti/Au electrode on Al_2O_3 in Buffer solution, (d) CV scan of Ti/Au electrode on Al_2O_3 with a UiO-66-NH_2 PLD coating.

Figure 3.6 (a) shows a series of measurements taken at their respective concentrations. The range of concentrations was such that 0.1 µg/L to 500 µg/L. Gold in this case shows no detection below 10 µg/L. Figure 3.6 (b) contains a more complex approach with the use of a 24 hour soaking period in the solution containing the analyte of choice, with magnetic stirring for the entiriety of the adsorption soak period. Then there is a short accumulation period followed by the stripping of the analyte. This figure shows the failure of the electrode design with the detection of lead at the electro chemical potential for gold to lead rather than carbon to lead. This correlates directly with what is seen in the CV scan. Figure 3.6 (c) are plots of control Ti/Au electrodes placed into the solution with the UiO-66-NH_2 PLD samples proving that there was no adsorption to the surface of the gold.

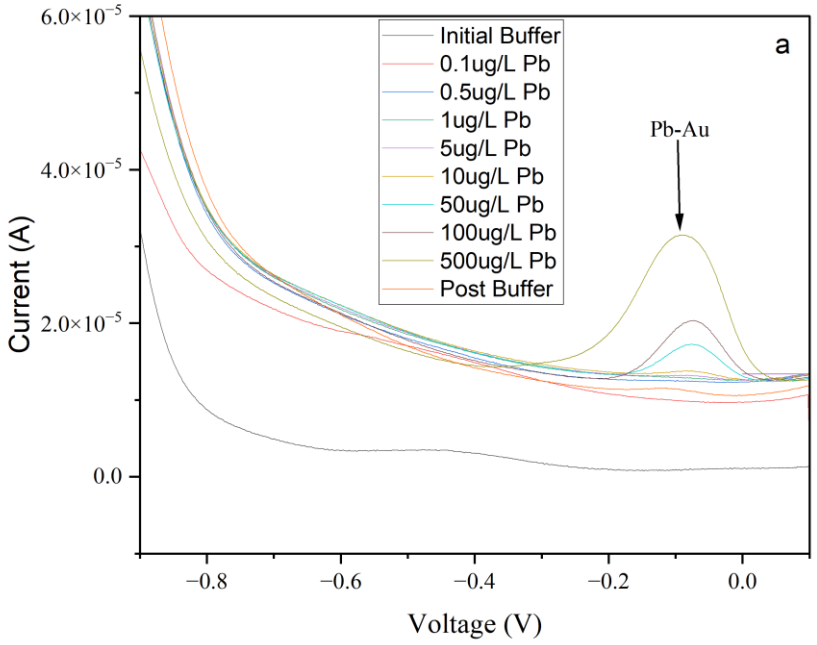

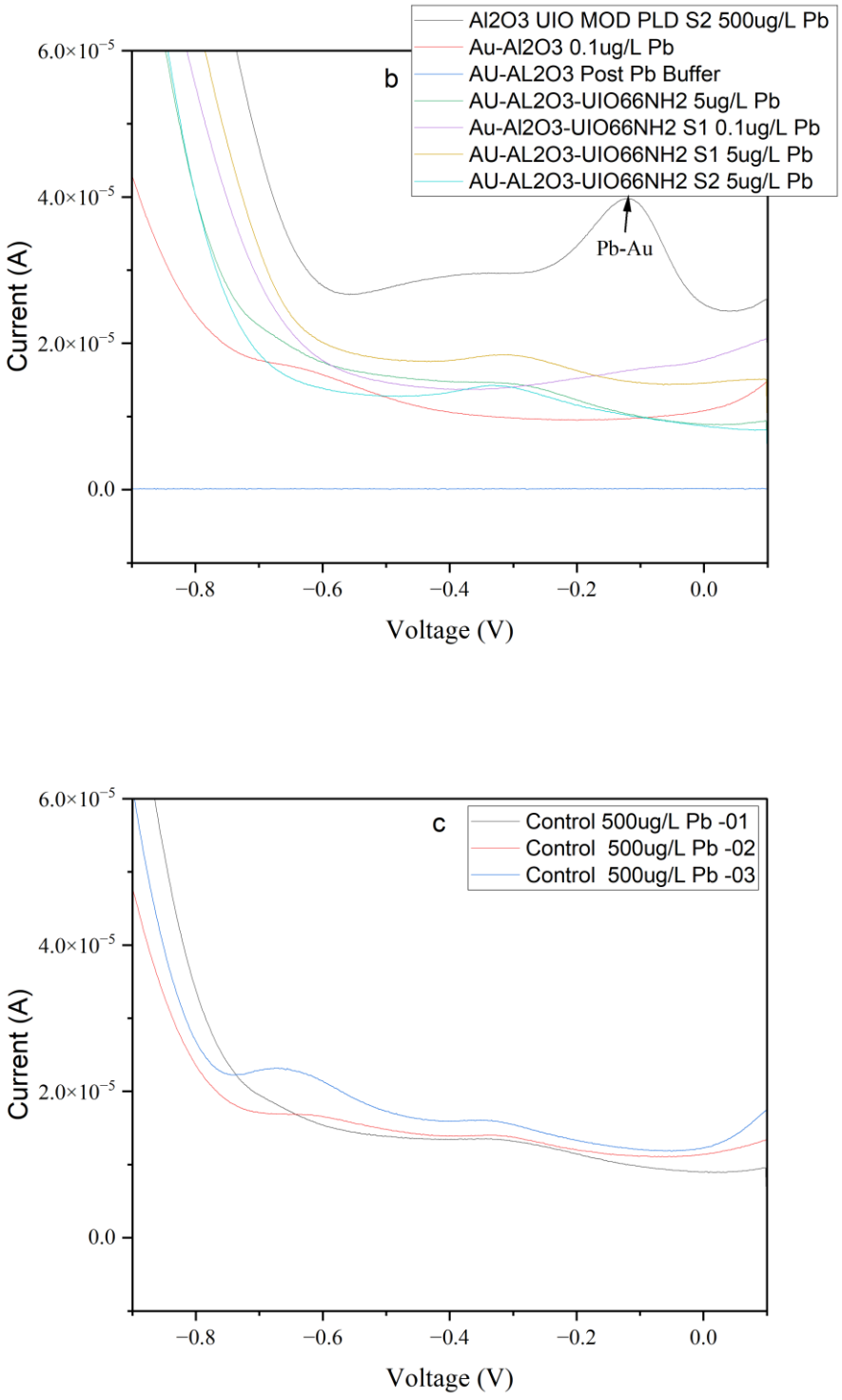

Figure 3.6: Square-wave anodic stripping voltammetry plots, (a) Ti/Au bare electrode tested for Pb^{2+} detection, (b) PLD grown MOF on the Ti/Au working electrode tested for Pb^{2+}, (c) Ti/Au tested with the same method as the MOF device.

Conclusion

Ti/Au is known to be an electrochemically stable elctrode in a wide variety of solutions, thus why it was chosen for this research. Sputtering of the electrode and its strong adhesion to the alumina substrate with the adiquite thickness of the titanium adhesion layer prove the process successful. Fourier transform infared spectroscopy done on the PLD film grown gives high confidence in the approach to a high quality thin film device development. Film thickness was analyzed with a laser scanning confocal microscope confirming that there was the desired thickness to the working electrode. The film thickness of the PLD grown film was also measured to insure full coverage of the electrode. Both cylic voltammetry and square-wave anodic stripping voltammetry were taken. The Ti/Au electrode matched properly with literature for both the CV and the SWSV scans. There was a mistake in not taking into account that there could be delamination of the PLD grown MOF, UiO-66-NH2, as there are resources suggesting this could be the case.

References

[1] Wang, Yang, et al. "A Metal–Organic Framework and Conducting Polymer Based Electrochemical Sensor for High Performance Cadmium Ion Detection." Journal of Materials Chemistry A, vol. 5, no. 18, 2017, pp. 8385–8393, doi:10.1039/c7ta01066d.

[2] Ibrahim, A. H., El-Mehalmey, W. A., Haikal, R. R., Safy, M. E. A., Amin, M., Shatla, H. R., Karakalos, S. G., & Alkordi, M. H. (2019). Tuning the Chemical Environment within the UiO-66-NH2 Nanocages for Charge-Dependent Contaminant Uptake and Selectivity. Inorganic Chemistry, 58(22), 15078–15087. https://doi.org/10.1021/acs.inorgchem.9b01611

[3] Saleem, H., Rafique, U., & Davies, R. P. (2016). Investigations on post-synthetically modified UiO-66-NH2 for the adsorptive removal of heavy metal ions from aqueous solution. Microporous and Mesoporous Materials, 221, 238–244. https://doi.org/10.1016/j.micromeso.2015.09.043

[4] Ru, J., Wang, X., Cui, X., Wang, F., Ji, H., Du, X., & Lu, X. (2021). GaOOH-modified metal-organic frameworks UiO-66-NH2: Selective and sensitive sensing four heavy-metal ions in real wastewater by electrochemical method. Talanta, 234, 122679. https://doi.org/10.1016/j.talanta.2021.122679

[5] Chu, J., Chu, B., Lu, C., Gu, Q., Li, W., Lin, R., Lu, J., & Chen, X. (2022). Highly sensitive detection of lead ions and cadmium ions based on UiO-66-NH2@carbon nanohorns composites enhanced by bismuth film in water environment. Journal of Environmental Chemical Engineering, 10(6), 108753. https://doi.org/10.1016/j.jece.2022.108753

[6] Pei, L., Yang, H., Chen, S., & Wang, L. (2022). UiO-66-NHC(S)NHMe/Three-Dimensional Macroporous Carbon for Removal and Electrochemical Detection of Cd2+, Pb2+, Cu2+, and Hg2+. Industrial & Engineering Chemistry Research, 61(4), 1588–1595. https://doi.org/10.1021/acs.iecr.1c04029

[7] Tu, X., Li, X., Liu, B., Zhai, C., Peng, Y., Wang, B., Hu, Z., Su, Z., & Qin, X. (2023). Facile one-pot synthesis of triethanolamine-functionalized AuNPs-GO-UiO-66-NH2 nanocomposites for simultaneous electrochemical detection of Cd(II), Pb(II), and Cu(II). Journal of Solid State Electrochemistry. https://doi.org/10.1007/s10008-023-05697-2

[8] Kuśmierek, K., & Świątkowski, A. (2015). The influence of different agitation techniques on the adsorption kinetics of 4-chlorophenol on granular activated carbon. Reaction Kinetics, Mechanisms and Catalysis, 116(1), 261–271. https://doi.org/10.1007/s11144-015-0889-1

[9] Rooney, M. B., Coomber, D. C., & Bond, A. M. (2000). Achievement of Near-Reversible Behavior for the [Fe(CN)6]3-/4- Redox Couple Using Cyclic Voltammetry at Glassy Carbon, Gold, and Platinum Macrodisk Electrodes in the Absence of Added Supporting Electrolyte. Analytical Chemistry, 72(15), 3486–3491. https://doi.org/10.1021/ac991464m

[10] Lahiri, B., Dylewicz, R., Rue, R. M. D. L., & Johnson, N. P. (2010). Impact of titanium adhesion layers on the response of arrays of metallic split-ring resonators (SRRs). Optics Express, 18(11), 11202–11208. https://doi.org/10.1364/OE.18.011202

[11] Guo, J., Fan, X., Wang, J., Yu, S., Laipan, M., Ren, X., Zhang, C., Zhang, L., & Li, Y. (2021). Highly efficient and selective recovery of Au(III) from aqueous solution by bisthiourea immobilized UiO-66-NH2: Performance and mechanisms. Chemical Engineering Journal, 425, 130588. https://doi.org/10.1016/j.cej.2021.130588

[12] Tang, J., Chen, Y., Wang, S., & Zhang, L. (2021). Engineering of UiO-66-NH2 as selective and reusable adsorbent to enhance the removal of Au(III) from water: Kinetics, isotherm and thermodynamics. Journal of Colloid and Interface Science, 601, 272–282. https://doi.org/10.1016/j.jcis.2021.05.121

[13] Zhao, M., Huang, Z., Wang, S., Zhang, L., & Wang, C. (2020). Experimental and DFT study on the selective adsorption mechanism of Au(III) using amidinothiourea-functionalized UiO-66-NH2. Microporous and Mesoporous Materials, 294, 109905. https://doi.org/10.1016/j.micromeso.2019.109905

Chapter 4: Summary

UiO-66-NH_2 thin films were successfully grown on various substrates and characterized for confirmation. XPS and FTIR showed promising results as to the chemical state and composition of the grown films. With the use of PLD in an inert environment at 100C the best film was able to be created. Electrical measurements prove that the film is insulating with dielectric measurements suggesting that the film has some porosity or saffolding structure, that would give it the framework desired. With the use of XPS and FTIR data a correlation was made to improve the film, the development of the modified method. This created a film that more closely matched that of the prisine UiO-66-NH_2. Development of an application was done, an electrochemical sensor for heavy metals in water. A Ti/Au working electrode was sputtered on an alumina substrate, SiO_2 failed, followed by the PLD MOF. The working electrode was a thickness of 114nm with a titanium adhesion layer of approximately 9 nm measured with ellipsometry, and the overall thickness measured with LSCM. The sensor itself was also analysed using LSCM for thickness. The sensor was tested for CV and SWSV and showed to delaminate, thus making the test invalid. Future work would include a change in working electrode to one that would have better adhesion.